

Formation of Zerovalent Iron in Iron-Reducing Cultures of *Methanosarcina barkeri*

Haitao Shang,* Mirna Daye, Orit Sivan, Caue S. Borlina, Nobumichi Tamura, Benjamin P. Weiss, and Tanja Bosak



Cite This: *Environ. Sci. Technol.* 2020, 54, 7354–7365



Read Online

ACCESS |



Metrics & More

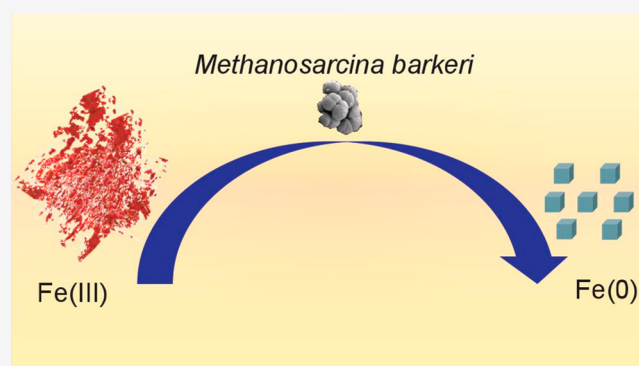


Article Recommendations



Supporting Information

ABSTRACT: Methanogenic archaea have been shown to reduce iron from ferric [Fe(III)] to ferrous [Fe(II)] state, but minerals that form during iron reduction by different methanogens remain to be characterized. Here, we show that zerovalent iron (ZVI) minerals, ferrite [α -Fe(0)] and austenite [γ -Fe(0)], appear in the X-ray diffraction spectra minutes after the addition of ferrihydrite to the cultures of a methanogenic archaeon, *Methanosarcina barkeri* (*M. barkeri*). *M. barkeri* cells and redox-active, nonenzymatic soluble organic compounds in organic-rich spent culture supernatants can promote the formation of ZVI; the latter compounds also likely stabilize ZVI. Methanogenic microbes that inhabit organic- and Fe(III)-rich anaerobic environments may similarly reduce Fe(III) to Fe(II) and ZVI, with implications for the preservation of paleomagnetic signals during sediment diagenesis and potential applications in the protection of iron metals against corrosion and in the green synthesis of ZVI.



1. INTRODUCTION

Microorganisms mediate numerous redox transformations of iron in natural environments and couple the biogeochemical cycles of iron, carbon, oxygen, sulfur, nitrogen, and other elements.^{1–4} In soils and sediments, microbes can utilize ferric iron [Fe(III)] as the electron acceptor for dissimilatory iron reduction.^{1,4,5} The reduction of Fe(III) produces ferrous iron [Fe(II)] that can be incorporated into different Fe(II)-containing minerals such as magnetite,^{6,7} vivianite,^{8,9} and siderite.^{10,11} The formation of specific mineral phases is thought to depend on pH, electron donors, $p\text{CO}_2$, and other environmental factors.¹¹

Methanosarcina barkeri (*M. barkeri*), a coccoid methanogen, can grow on methanol, acetate, and carbon dioxide/hydrogen.^{12,13} The growth physiology of *M. barkeri* depends on the redox potential of the ambient environment: this microbe is able to survive high redox-potential conditions by generating its own low potential environment.¹⁴ When *M. barkeri* produces methane (CH_4) with hydrogen gas (H_2) as the electron donor, it uses several electron carriers with low redox-potentials such as ferredoxin ($E^{0'} = -500$ mV), coenzyme F₄₂₀ ($E^{0'} = -360$ mV), coenzyme B ($E^{0'} = -140$ mV), and methanophenazine ($E^{0'} = -165$ mV).¹⁵ These enable *M. barkeri* to reduce a range of oxidized compounds including ferrihydrite [$\text{FeOOH}(\text{am}) \rightarrow \text{Fe}(\text{II})$, $E^{0'} = -50$ mV¹⁶] into products with rather low reduction potentials. *M. barkeri* has been shown to reduce amorphous^{17–19} and crystalline^{20,21}

Fe(III) to Fe(II). Some of these studies also reported the formation of iron minerals such as magnetite¹⁹ and vivianite.²⁰ However, only mineral phases that contain Fe(III) and/or Fe(II) have been reported, although other minerals, such as ilmenite, were hypothesized as well.¹⁷

The low redox-potential environments where *M. barkeri* grows and persists may support the formation of other iron phases with low reduction potential, such as zerovalent iron (ZVI) [$\text{Fe}(\text{III}) + 3e^- \rightarrow \text{Fe}(\text{0})$, $E^{0'} = -37$ mV²²]. ZVI is unstable in most surface environments because it is easily oxidized to Fe(II) or Fe(III) by both abiotic²³ and biological^{24–27} reactions in a process known as iron corrosion. The reverse process—that is, the reduction of oxidized iron to ZVI—has also been observed in some abiotic reactions.^{28–31} One example is the formation of Fe(0) in awaruite, a nickel and iron-containing alloy, in serpentinizing environments.³¹ Several studies have also reported the reduction of Fe(III) in aqueous tea-leaf extracts to ZVI.^{32–34} However, to the best of our knowledge, only one study reported the presence of small X-ray diffraction peaks of Fe(0) in microbial enrichment

Received: March 13, 2020

Revised: May 3, 2020

Accepted: May 7, 2020

Published: May 7, 2020



Table 1. Experimental Design

# bottle	<i>M. barkeri</i>	Fe(III) source	timing of Fe(III) addition	headspace	organics (g/L)	reductant	separation	heating
1, 2, 3	inoculated	ferrihydrite	exponential phase	N ₂ /CO ₂	1.0	Ti(III)-citrate	no	no
4, 5, 6	inoculated	ferrihydrite	stationary phase	N ₂ /CO ₂	1.0	Ti(III)-citrate	no	no
7, 8, 9	inoculated	ferrihydrite	exponential phase	CH ₄ /H ₂ /CO ₂	1.0	Ti(III)-citrate	no	no
10, 11, 12	inoculated	ferrihydrite	stationary phase	CH ₄ /H ₂ /CO ₂	1.0	Ti(III)-citrate	no	no
13, 14, 15	inoculated	ferrihydrite	exponential phase	N ₂ /CO ₂	4.0	Ti(III)-citrate	no	no
16, 17, 18	inoculated	ferrihydrite	stationary phase	N ₂ /CO ₂	4.0	Ti(III)-citrate	no	no
19, 20, 21	sterile control	ferrihydrite		N ₂ /CO ₂	1.0	Ti(III)-citrate	no	no
22, 23, 24	sterile control	ferrihydrite		CH ₄ /H ₂ /CO ₂	1.0	Ti(III)-citrate	no	no
25, 26, 27	sterile control	ferrihydrite		N ₂ /CO ₂	4.0	Ti(III)-citrate	no	no
28, 29, 30	inoculated	ferrihydrite	exponential phase	N ₂ /CO ₂	1.0	L-cysteine	no	no
31, 32, 33	sterile control	ferrihydrite		N ₂ /CO ₂	1.0	L-cysteine	no	no
34, 35, 36	procedure control	ferrihydrite	exponential phase	N ₂ /CO ₂	1.0	Ti(III)-citrate	yes	no
37, 38, 39	inoculated	ferrihydrite	exponential phase	N ₂ /CO ₂	organic-free	Ti(III)-citrate	yes	no
40, 41, 42	filtrate (no cells)	ferrihydrite	exponential phase	N ₂ /CO ₂	1.0	Ti(III)-citrate	yes	no
43, 44, 45	inoculated	ferrihydrite	exponential phase	N ₂ /CO ₂	organic-free	Ti(III)-citrate	yes	yes
46, 47, 48	filtrate (no cells)	ferrihydrite	exponential phase	N ₂ /CO ₂	1.0	Ti(III)-citrate	yes	yes
49, 50, 51	sterile control	ferrihydrite		N ₂ /CO ₂	organic-free	Ti(III)-citrate	yes	no
52, 53, 54	sterile control	ferrihydrite		N ₂ /CO ₂	organic-free	Ti(III)-citrate	yes	yes
55, 56, 57	inoculated	FeCl ₃	exponential phase	N ₂ /CO ₂	1.0	Ti(III)-citrate	no	no
58, 59, 60	sterile control	FeCl ₃		N ₂ /CO ₂	1.0	Ti(III)-citrate	no	no

cultures of *Geobacter sulfurreducens* and *Shewanella denitrificans* that grew on ochre pigment.³⁵

Here, we explore the biomineralization of iron in low-potential environments that support microbial methanogenesis. This is done by characterizing minerals that form in iron-reducing cultures of *M. barkeri* and exploring mechanisms that produce and stabilize these minerals. Our results demonstrate the formation of titanomagnetite (or magnetite) and ZVI in active *M. barkeri* cultures and spent culture supernatants. The ability of *M. barkeri* to reduce oxidized iron to its metallic state may influence the cycling of nutrients and toxins in the environments, with potential applications in the protection against iron corrosion and in the green synthesis of ZVI.

2. MATERIALS AND METHODS

2.1. Cell Incubation. *M. barkeri* (DSM 800) was obtained from Deutsche Sammlung von Mikroorganismen und Zellkulturen (DSMZ, Braunschweig, Germany). All serum bottles (160 mL) were autoclaved at 120 °C for 30 min. Media were prepared according to modified medium recipe (Oregon Collection of Methanogens Medium for Methanogens¹⁷) (Supporting Information, SI, Table S1). The medium contained either a low organic content (1.0 g/L of 50/50 wt % yeast extract and casitone, DIFCO) or a high organic content (4.0 g/L of 50/50 wt % yeast extract and casitone, DIFCO). Organic-free medium was prepared according to the same recipe, but without yeast extract and casitone. The media were titrated with a saturated NaHCO₃ solution to pH 6.8. All media were prepared anaerobically, filter sterilized, and added into the autoclaved serum bottles. *M. barkeri* cannot grow in the presence of O₂, so the vacuum-vortex technique³⁶ was used to generate anaerobic conditions in the serum bottles. Gas mixture of H₂/CO₂ (80%/20%) was added into serum bottles as the headspace atmosphere. Each 160 mL serum bottle contained 50 mL of liquid and 110 mL of headspace gas. The final pressure of the headspace atmosphere was 100 kPa. Either Ti(III)-citrate (2.56 mM final concentration) or L-cysteine (0.5 mM final concentration) was used as reducing agent. Sulfide was not used as a reducing agent to avoid reactions with iron

species and the formation of sulfide minerals. Preliminary experiments used different final concentrations of Ti(III)-citrate (0.85 mM, 2.56 mM and 7.67 mM) and found that 2.56 mM Ti(III)-citrate was optimal for *M. barkeri* to grow and produce CH₄. All cultures and controls were incubated at 37 °C.

2.2. Experimental Design. The experimental design is summarized in Table 1. Initially, we explored the biomineralization in *M. barkeri* cultures in the presence of ferrihydrite as a function of the following: (1) the content of organic additives in medium, (2) the timing of ferrihydrite addition, and (3) the composition of headspace gas in serum bottles. The *M. barkeri* inocula for all experiments were grown in the medium with 1 g/L organic additives, these cultures were inoculated at 1:10 v/v into media that contained either 1 g/L or 4 g/L organic additives for growth and/or iron-reduction experiments. Most experiments described in what follows used 1 g/L of these additives (yeast extract and casitone), a 4-fold reduction relative to 4 g/L in the original recipe.¹⁷ Poorly crystalline ferrihydrite was prepared by titrating FeCl₃ with 10N NaOH to pH 7 to a final concentration of 7.5 mM of ferrihydrite. Before the addition of ferrihydrite, the headspaces of triplicate *M. barkeri* cultures and triplicate sterile controls were flushed by N₂/CO₂ (80%/20%) for 1 h. To test if the headspace gas composition influences the precipitation of Fe(0), the headspaces of additional serum bottles with triplicate *M. barkeri* cultures or sterile media were not flushed to remove H₂ and CH₄. Aqueous FeCl₃ (7.5 mM final concentration) was added to the *M. barkeri* cultures to test the influence of a different iron source on the production of Fe(0).

Precipitates formed in *M. barkeri* cultures and sterile controls were sampled 30 min, 28 days, and 42 days after the addition of ferrihydrite. X-ray powder diffraction (XRD) and microfocused X-ray diffraction (μ XRD) were used to characterize the mineral phases in the precipitates. Scanning electron microscopy (SEM) was used to observe the morphology of *M. barkeri* cells, minerals and characterize the association of cells and minerals. Energy-dispersive X-ray spectroscopy (EDS) was used to determine the elemental

composition of solids in the cultures. The redox state of iron was measured by X-ray photoelectron spectroscopy (XPS). The concentration of Fe(II) was quantified by ferrozine assay.³⁷ The composition of headspace gases was characterized using gas chromatography.

To test the effects of soluble electron donors on the reduction of iron from ferric to metallic state, we separated *M. barkeri* cells and supernatants before the addition of ferrihydrite. This procedure consisted of the following steps: (1) cells were separated from medium by filtration using 0.1 μm pore-size filters (glass microfiber, Cole Parmer, IL, U.S.A.); (2) spent supernatants were placed into clean, autoclaved, and anaerobic serum bottles; (3) cells were washed with anoxic nanopure water; (4) cells were transferred into fresh organic-free medium in autoclaved and anaerobic serum bottles; (5) headspaces were flushed by N_2/CO_2 (80%/20%) for 1 h; and (6) ferrihydrite was added to the serum bottles that contained either filtered spent supernatants or cells in fresh organic-free medium. All steps in this procedure were performed using the sterile technique in an anaerobic glovebox. To ascertain that the separation process did not influence the physiology of *M. barkeri*, procedure control cultures contained cells that were added back to the filtered spent supernatants after the filtration and before the addition of ferrihydrite.

To determine whether any transient mineral phases formed in the early stages of these experiments, precipitates from cells and supernatants were sampled for XRD characterization at 1 min, 5 min, 10 min, and 30 min after the addition of ferrihydrite. After 30 min, the precipitates were sampled for analysis every 14 days until 42 days after the addition of ferrihydrite. Iron concentrations were measured at each sampling point.

To explore the roles of extracellular and cell-associated enzymes in the reduction of ferrihydrite and the production of Fe(0), we followed above procedure [steps (1) to (4)] to separate *M. barkeri* cells and supernatants, flushed the headspaces by N_2/CO_2 (80%/20%) for 1 h, heated all serum bottles and organic-free sterile controls to 120 °C for 4 h and allowed them to cool down for 5 h to room temperature (20 °C) before the addition of ferrihydrite.

Because some reducing agents such as Ti(III)-citrate were previously hypothesized to influence the redox transformations of iron,¹⁷ we also tested the importance of this reductant for the formation of Fe(0). This was done by replacing Ti(III)-citrate by L-cysteine (0.5 mM final concentration) as the reducing agent in the medium with low organic content (1 g/L).

2.3. Analytical Methods. The concentrations of headspace gases, including CH_4 , CO_2 , and H_2 , were measured in triplicate by a Shimadzu GC-2014 gas chromatograph configured with a packed column (Carboxen-1000, 5' \times 1/8", Supelco, Bellefonte, Pennsylvania, U.S.A.). The temperature was set to 140 °C, and argon was used as the carrier gas. CH_4 and CO_2 were measured by the methanizer-flame ionization detector (FID) and H_2 was measured by the thermal conductivity detector (TCD). The concentrations of gases were calculated from their partial pressures based on the standards calibrated with the SCOTTY Specialty Gas (T237-14, Sigma-Aldrich Corporation, MO, U.S.A.).

The concentrations of Fe(II) were measured by a microplate reader (BioTek, Synergy 2, VT, U.S.A.) at 562 nm in 200 μL triplicate samples of mixtures obtained by mixing 1 mL subsamples of media that had been filtered through 0.2 μm

pore-size filters (Acrodisc 25 mm syringe filter, PALL Corporation, MA, U.S.A.) and fixed immediately with 100 μL ferrozine solution. This solution was prepared by dissolving 0.01 M ferrozine (FW 492.47, 97%) in 0.1 M ammonium acetate ($\text{CH}_3\text{COONH}_4$, 99.99%) solution.³⁷ The concentrations of Fe(II) were determined using standards that contained solutions of Fe(II) with known concentrations from 0 to 0.36 mM and analytical standard deviation of ~ 0.001 mM. The reported errors in this paper are the standard deviations from the measured triplicates.

Precipitated minerals were characterized using XRD on an X'Pert PRO diffractometer (PANalytical manufacturer) equipped with an X'Celerator detector. The precipitates were collected by centrifugation at 14 000 rpm for 5 min, smeared on zero diffraction disk (23.6 mm diameter \times 2.0 mm thickness, Si Crystal, MTI Corporation, CA, U.S.A.) and dried in an anaerobic glovebox. The samples were analyzed inside an anaerobic dome to maintain the anoxic conditions during the XRD analyses. The XRD patterns were measured in reflection mode with nickel-filtered copper $K\alpha$ radiation ($\lambda = 1.5406$ Å) as the X-ray source. The X-ray energy and the wavelength, respectively, were set with a Si(III) double-crystal monochromator to be, respectively, 10 keV and 1.2404 (± 0.001) Å. The 2θ angle ranged from 3° to 90° with a scanning step of 0.008°. The fixed counting time was set as 1000 s at 45 kV and 40 mA. Wavelength and 2θ calibrations were maintained by frequently measuring intensity data from an aluminum foil (transmission geometry) or LaB6 powder (reflection geometry). A platinum-coated toroidal focusing mirror with a step size of 0.04° was used to reject X-rays with the energies > 11 keV and to produce a focused beam of dimensions 1 \times 4 mm². Transmission data were corrected for θ -dependent attenuation of incident and scattered X-rays. XRD spectra were analyzed with the High Score Plus program (version 4.5, Malvern Panalytical Incorporated, Netherlands). Rietveld fitting method³⁸ was used to refine crystals and to determine the atomic coordinates and lattice parameters of different mineral phases. Iron phases were determined according to the Miller indices (hkl) that denote planes orthogonal to the reciprocal crystal lattice vector. The presence of superstructure reflections (hkls of 111 and 200) at $2\theta = 42.94^\circ$ and 50.01° indicated austenite [$\gamma\text{-Fe(0)}$] with the d -spacing of 2.104 Å. The presence of superstructure reflections (hkls of 110, 200 and 211) at $2\theta = 45.32^\circ$, 66.03° and 83.72° indicated ferrite [$\alpha\text{-Fe(0)}$] with the d -spacing of 1.999 Å. Rietveld fitting was also used to quantify the phases in the fitting phase mixture and determine the percentages of austenite and/or ferrite.

Minerals were also analyzed using in situ synchrotron μXRD at the Advanced Light Source (Lawrence Berkeley National Laboratory, CA, U.S.A.) at the beamline 12.3.2. Samples were collected on site, and the sample paste was loaded into transmission sample XRD cells. The transmission synchrotron diffraction data were collected using a DECTRIS Pilatus 1 M hybrid pixel area detector placed at $2\theta = 35^\circ$ at approximately 170 mm from the sample. The 4-bounce monochromator was set to 10 keV ($\lambda = 1.239842$ Å). The sample geometry with respect to the incident beam and the detector was calibrated using Al_2O_3 powder. The 2D diffraction patterns were analyzed and integrated along the azimuthal direction into 1D diffractograms using the X-ray microdiffraction analysis software (version 6, XMAS) developed at the Advanced Light Source for the beamline 12.3.2, and MATLAB R2017a.

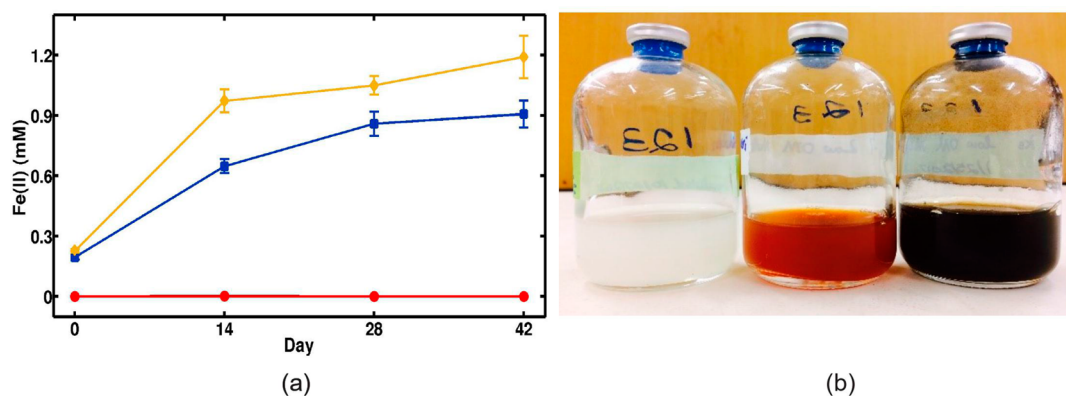


Figure 1. Representative changes of Fe(II) concentration and color in iron-reducing cultures of *M. barkeri* and sterile controls. The headspaces of all cultures and controls shown here contained N_2/CO_2 . The medium in all *M. barkeri* cultures and controls contained 1.0 g/L of yeast extract and casitone. (a) Fe(II) concentration. Blue line and squares show measurements from *M. barkeri* cultures to which ferrihydrite was added in exponential phase. Yellow line and diamonds show measurements from *M. barkeri* cultures to which ferrihydrite was added in stationary phase. Red line and circles show that Fe(II) was not produced in sterile controls. Each time point shows the average concentration from triplicate bottles and the error bars show the standard deviation. (b) Representative color changes in cultures and sterile controls. Left (white) bottle contains *M. barkeri* without ferrihydrite, the middle (reddish) bottle is the sterile control and the right (black) bottle contains *M. barkeri* incubated with ferrihydrite for 28 days.

XPS was performed on a K-Alpha X-ray photoelectron spectrometer (Thermo Fisher Scientific, MA, U.S.A.). All samples were fractured in high vacuum (3×10^{-8} Torr) in the Kratos outer pressure chamber and then moved directly into the main XPS measurement chamber. An incident monochromatic X-ray beam from the Al K Alpha target (10 kV, 10 mA) was focused on a 0.4×0.3 mm² area at a 45° angle with respect to the sample surface. The electron energy analyzer perpendicular to the sample surface was operated with a pass energy of 50 eV to obtain XPS spectra at a 0.1 eV step size and a dwell time of 50 ms. Each peak was scanned 15 times. To ensure representative data from heterogeneous samples, we probed a total of 50–70 points per sample. XPS data were treated and analyzed using CasaXPS curve resolution software package. Spectra were best fit after Shirley background subtractions by nonlinear least-squares CasaXPS curve resolution software package. Gaussian/Lorentzian contributions to the line shapes were numerically convoluted using a Voigt function. The different XPS lines with sets of Gaussian and Lorentzian peaks were empirically fitted with different standards corresponding to different states—Fe(0), Fe(II), and Fe(III).

Thermomagnetic measurements were attempted to quantify the amount of ZVI in the samples. This was done by heating the samples to a temperature at which only ZVI contributes significantly to the magnetization. In particular, if the samples are heated up to the titanomagnetite Curie temperature (<580 °C), then the saturation magnetic moment at this temperature could be used to infer the amount of ZVI given knowledge of ZVI's temperature-dependent saturation magnetization [eq (2) in ref 39]. With this goal, we sampled the precipitates from exponential-phase *M. barkeri* cultures incubated in high organic medium (4 g/L) under a N_2/CO_2 headspace and placed ~0.1 mL samples on top of a MicroSense quartz perpendicular sample holder (blank saturation magnetic moment of 4×10^{-9} Am²). The samples were left to dry inside an anaerobic glovebox. We then acquired saturation magnetization thermomagnetic measurements using an ADE model 1660 vibrating sample magnetometer with an applied field of 1 T at intervals of 50 °C from room temperature up to 350 °C (C.

Ross Laboratory in the Department of Materials Science and Engineering at MIT, MA, U.S.A.). Both heating and cooling curves were obtained to check for thermochemical alteration.

SEM was used to image microbial and mineral morphologies, and microbe-mineral associations. Scanning electron micrographs were acquired by a Zeiss Merlin GEMINI II column high-resolution scanning electron microscope (Carl Zeiss microscopy, CA, U.S.A.) equipped with a field gun emission and EDS (EDAX detector; EDAX, NJ, U.S.A.) operating at an accelerating voltage of 5–15 kV, probe current of 100 pA and a working distance of 8.5 mm. On-axis in-lens secondary electron (SE-mode) detector was used during imaging. The samples were fixed by 0.2 M sodium cacodylate, 0.1% $CaCl_2$ and 2.5% glutaraldehyde in anaerobic water for 2–3 days at 4 °C. The fixed samples were washed by 0.1 M sodium cacodylate, followed by a wash in nanopure water. After washing, the samples were dehydrated with a series of ethanol–water solutions consisting of 30% (20 min), 50% (20 min), 70% (20 min), 80% (20 min), 90% (20 min), and 100% (20 min) of 200 proof ethanol. After air-drying, the samples were mounted on double-sided carbon tape and coated with a thin layer 5 nm of Au/Pd or 10 nm of carbon before imaging using Hummer V sputter coater. EDS spectra were treated and analyzed using TEAM EDS software (version 2.0, EDAX Incorporated, NJ, U.S.A.) and Microsoft Excel 2016.

3. RESULTS

Because ferrihydrite is a common form of Fe(III) in the environment,⁴⁰ we used this phase as the solid electron acceptor in most of our experiments. We explored the formation of iron minerals in *M. barkeri* cultures by adding ferrihydrite to the cultures initially grown on H_2/CO_2 . The concentration of Fe(II) in cultures increased with the incubation time due to the continuous reduction of ferrihydrite [Figure 1(a)], regardless of the growth phase and the composition of the headspace gases (Table 1). The color of the medium darkened with the incubation time and black precipitates formed [Figure 1(b)].

Precipitates were first sampled from cultures and sterile controls 30 min after the addition of ferrihydrite. Figure 2

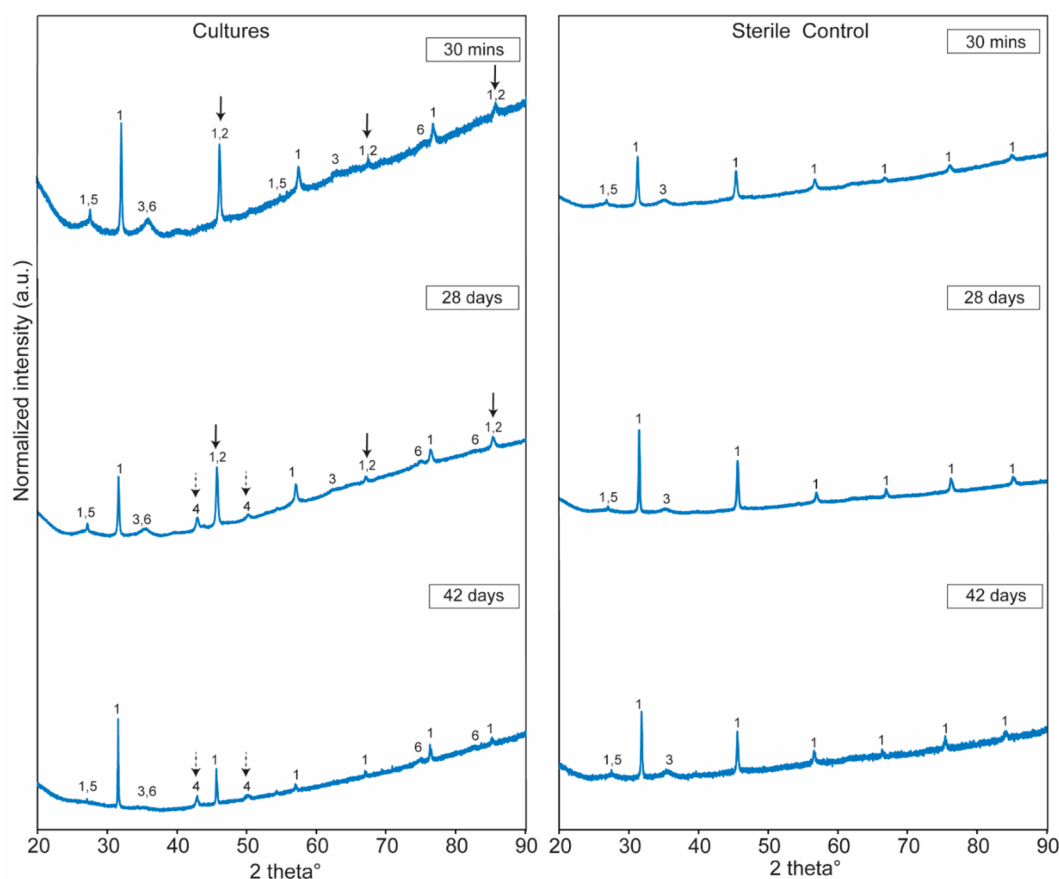


Figure 2. XRD spectra of minerals sampled from *M. barkeri* cultures (left column) and sterile controls (right column). The medium was reduced by Ti(III)-citrate and contained 1 g/L of organic additives. The headspace gas was replaced by N_2/CO_2 before the addition of ferrihydrite in exponential phase. The samples were collected at 30 min, 28 days and 42 days after the addition of ferrihydrite. XRD peak assignments: (1) Halite (NaCl); (2) Ferrite [α -Fe(0)]; (3) Ferrihydrite (Fe_2O_3); (4) Austenite [γ -Fe(0)]; (5) Rutile (TiO_2); and (6) Titanomagnetite ($Ti_2Fe_3O_4$).

shows representative XRD data. At this time point, halite (NaCl) and rutile (TiO_2) were present in the XRD spectra of both *M. barkeri* cultures and sterile controls. This showed that rutile formed by the abiotic oxidation of Ti(III)-citrate. Fe(II)-containing titanomagnetite ($Ti_2Fe_3O_4$) was observed in *M. barkeri* cultures at all sampling time points, but never in sterile controls. Surprisingly, the *M. barkeri* cultures at 30 min also contained ferrite [α -Fe(0)] with d -spacing of 1.999 Å. Because the α -Fe(0) and halite peaks overlapped, we used the Rietveld refinement to show that α -Fe(0) was indeed present (SI Table S2). After 28 days, the peaks of austenite [γ -Fe(0)] with d -spacing of 2.104 Å appeared in *M. barkeri* cultures. After 42 days, the peaks of α -Fe(0) disappeared from the XRD spectra, but the peaks of γ -Fe(0) were still present. γ -Fe(0) was also detected by μ XRD (SI Figure S1) and XPS (SI Figure S2). To confirm that Fe(0) was not present in the original iron source, we characterized ferrihydrite samples by XRD and found no Fe(0) peaks. These observations showed that ferrihydrite-reducing *M. barkeri* produced titanomagnetite and mediated the precipitation of Fe(0). The same phases were detected in *M. barkeri* cultures in stationary phase (SI Figure S3), under a $CH_4/H_2/CO_2$ atmosphere (SI Figure S4) and in the high-organic (4 g/L) medium (SI Figure S5). α -Fe(0) was absent from sterile controls at all times, whereas some low-intensity XRD peaks—either a single peak or two small peaks—matching γ -Fe(0) appeared in some spectra of sterile controls 28 days after the addition of ferrihydrite (SI Figures S4 and

S5). These Fe(0) peaks were detected in two-thirds of all independent experiments under these conditions and were not detectable 42 days after the addition of ferrihydrite. In contrast, γ -Fe(0) was always identifiable by two distinct peaks in the XRD spectra of *M. barkeri* cultures and remained detectable 42 days after the addition of ferrihydrite. If γ -Fe(0) was indeed present in sterile controls, then some components in the sterile media can contribute to the formation of Fe(0), but are not effective at stabilizing it over long incubation times.

The stoichiometry of the reduction of Fe(III) to Fe(II) and Fe(0) remains to be elucidated. Under our experimental conditions, titanomagnetite formed readily, so we were not able to separate various solid phases, quantify the relative amounts of reduced iron present in titanomagnetite and ZVI, and compare them to the concentrations of Fe(II) in the solution. Thermomagnetic measurements were used to determine the quantities of magnetite and Fe(0) (SI Figure S6); however, these attempts were not successful due to the production of new magnetic materials and changes in magnetic mineralogy during the laboratory heating cycle.

SEM imaging revealed morphological changes of *M. barkeri* and the morphologies of minerals that formed during the incubation with ferrihydrite. Initially, the rounded *M. barkeri* cells had smooth surfaces and formed large aggregates (SI Figure S7). After the addition of ferrihydrite, the diameter of *M. barkeri* cells and the sizes of cell aggregates decreased with the incubation time and the cells exhibited wrinkled surfaces

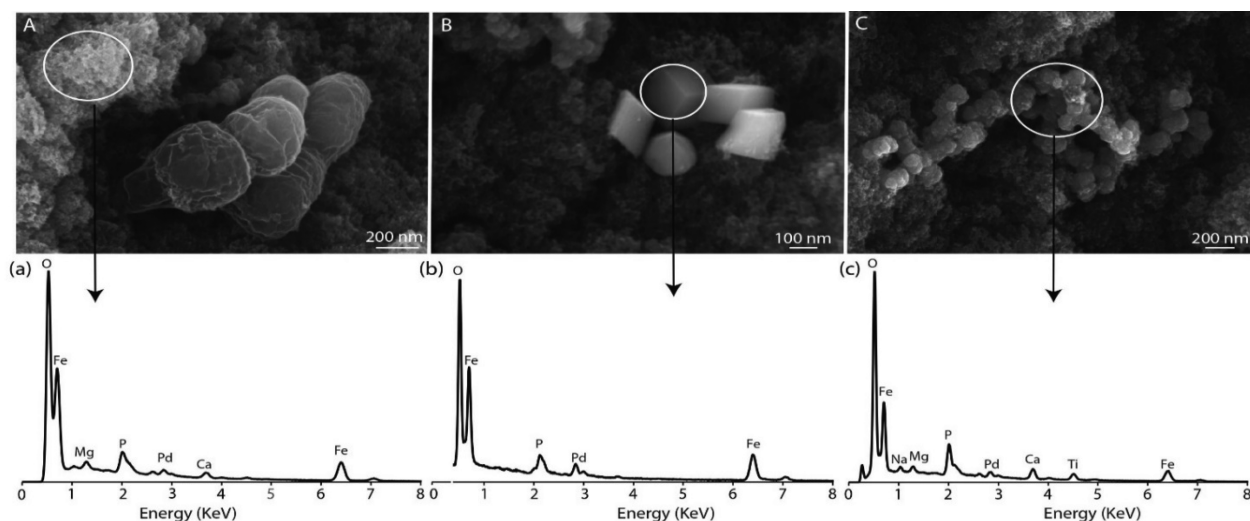


Figure 3. SEM images and EDS spectra of *M. barkeri* cultures and minerals 28 days after the addition of ferrihydrite. (A) Wrinkled surfaces of *M. barkeri*. (a) EDS spectrum of amorphous ferrihydrite. The peak of phosphorus (labeled as P) was also present in the EDS spectra of ferrihydrite from sterile controls. (B) Cubic-shaped ZVI. (b) EDS spectrum of (B). (C) Titanomagnetite. (c) EDS spectrum of (C).

[Figure 3(A)]. Cubic minerals with the EDS spectra consistent with ZVI phases and spherical minerals with the EDS spectra consistent with titanomagnetite were not associated with cells or cell aggregates [Figure 3(B) and (C)], suggesting that the formation of these minerals did not require direct cell–mineral contact.

To understand whether the precipitation of Fe(0) was a function of the Fe(III) source, we added aqueous FeCl₃ (7.5 mM final concentration) to the triplicate cultures of exponential-phase *M. barkeri* and triplicate sterile controls. All bottles contained medium with a low content (1 g/L) of organic additives and was reduced by Ti(III)-citrate. All headspaces were replaced by N₂/CO₂ before the addition of FeCl₃. Again, halite and rutile peaks were present in the XRD spectra of both *M. barkeri* cultures and sterile controls (SI Figure S8) at all time points. The precipitates in *M. barkeri* cultures also contained titanomagnetite, but α -Fe(0) peaks only appeared in these cultures 42 days after the addition of FeCl₃. ZVI was absent from the sterile controls at all time points. Thus, ZVI formed much more slowly when FeCl₃ was used instead of ferrihydrite as the source of ferric iron.

To determine the influence of reducing agents on the formation of Fe(0), we added 0.5 mM L-cysteine instead of Ti(III)-citrate to the medium with a low organic content (1 g/L). The headspace was replaced by N₂/CO₂ before the addition of ferrihydrite to exponential-phase cultures and sterile controls. The XRD spectra (SI Figure S9) showed Fe(0), magnetite and halite in the solids from the cysteine-reduced cultures. As expected, rutile and titanomagnetite were absent due to the lack of Ti(III). Thus, the formation of Fe(0) did not depend on the presence of Ti(III) as the reducing agent. The XRD spectra of cysteine-reduced sterile controls (SI Figure S9) contained α -Fe(0) at 28 days and γ -Fe(0) phase at 42 days after the addition of ferrihydrite. This observation was consistent with the previously reported ability of L-cysteine to precipitate and stabilize ZVI.⁴¹

We hypothesized that both *M. barkeri* cultures and dissolved electron donor(s) reduced iron.¹⁷ To understand the relative importance of either mechanism in the reduction of ferric iron and the formation of ZVI, we separated *M. barkeri* cells in exponential phase from the liquid medium by filtration. The

organic-free medium in sterile serum bottles was inoculated by these filter-separated cells. Equal volumes of organic-containing spent culture supernatants were added to three clean, autoclaved and anaerobic sterile serum bottles. The headspaces of all bottles were then flushed by N₂/CO₂ before the addition of ferrihydrite (Table 1). To confirm that the filtration did not influence the physiology of *M. barkeri*, we recombined the filtered *M. barkeri* cells and the filtered supernatants in a separate procedure control (Table 1). The final Fe(II) concentration in this procedure control was 0.86 mM. This recovered around 95% of the Fe(II) concentration—0.91 mM—measured in a previous experiment where the cells were not separated from the supernatants [Figure 1(a)] and showed that the filtration and separation of cells from the spent culture supernatants did not influence the physiology of *M. barkeri*. Iron reduction occurred both in the organic-free medium with *M. barkeri* cells and in filter-sterilized spent supernatants that lacked cells (Figure 4), but cells and organic additives reduce iron by different mechanisms and at different rates. Namely, the concentration of Fe(II) in the organic-free medium inoculated by *M. barkeri* increased to about 0.3 mM during the first 30 min after the addition of ferrihydrite (Figure 4) and remained unchanged afterward. In contrast, the filtered supernatants contained only 0.013 mM Fe(II) at 30 min after the addition of ferrihydrite, but the concentration of Fe(II) increased to 0.52 mM after 28 days (Figure 4). These differences between organic-free *M. barkeri* cultures and cell-free spent culture supernatants were accompanied by different trends in the formation and stabilization of ZVI.

Previous studies identified green rust, an unstable precursor of several iron oxide minerals such as magnetite and hematite, as a transient phase during iron reduction under both biotic and abiotic experimental conditions.^{42–44} To look for the presence of similar short-lived mineral phases in *M. barkeri* cultures, we sampled the precipitates from the organic-free medium inoculated by cells and filter-sterilized spent supernatants at 1, 5, 10, and 30 min after the addition of ferrihydrite. After that time, the samples were collected every 14 days. In short, we did not detect green rust in any of the analyzed precipitates, but did confirm various observations from our

previous experiments. In the organic-free medium inoculated by cells (Figure 5), peaks of α -Fe(0) appeared in the precipitates at 1 min after the addition of ferrihydrite. Their intensity decreased over the first 30 min of the experiment to below the detection limit after 14 days. Comparatively, smaller α -Fe(0) peaks appeared in the XRD spectra of the spent supernatants 1 min after the addition of ferrihydrite and their intensity increased at 5, 10, and 30 min (Figure 5). α -Fe(0) in the spent supernatants transformed to a different phase of ZVI— γ -Fe(0)—after 14 days, but none of the Fe(0) phases were detectable in 42-day-old samples. Again, because the α -Fe(0) and halite peaks overlapped, the Rietveld refinement was used to demonstrate the presence of α -Fe(0) (SI Table S3). Fe(0) minerals were absent from organic-free sterile controls at all time points (SI Figure S10). These experiments revealed the very rapid formation of Fe(0) when either *M. barkeri* cells were present in the organic-free medium or organic compounds were present in the cell-free spent supernatants. The stabilization of Fe(0) phases for more than 30 days required both cells and organic additives. We detected no Fe(0) in the organic-free sterile controls (SI Figure 10), but found tentative peaks in the sterile controls amended by organic compounds 28 days after the addition of ferrihydrite (SI Figures S4 and S5). Hence, yeast extract and casitone may promote the formation of ZVI, but are not sufficient for its stabilization.

Our results so far indicated that *M. barkeri* cells and soluble organic compounds both promoted the formation and stabilization of ZVI. To determine whether this process required some enzymatic activity, we characterized the precipitates from the heat-treated spent supernatants and the organic-free medium inoculated by *M. barkeri* cells. Spent supernatants or organic-free *M. barkeri* cultures were prepared as described in the previous paragraphs (also see Section 2.2). Triplicate sealed serum bottles containing either separate were heated at 120 °C in an oven for 4 h and allowed to cool at room temperature for 5 h before the addition of ferrihydrite. The heat-treated *M. barkeri* cultures reduced 0.007 mM of Fe(III) to Fe(II) 30 min after the addition of ferrihydrite; this concentration remained unchanged after 42 days (SI Figure S11). The concentration of Fe(II) in heat-treated spent supernatants increased from 0.005 mM at 30 min after the addition of ferrihydrite to 0.313 mM after 42 days (SI Figure S11). These concentrations were 2.5% and 64.3% of the respective Fe(II) concentrations measured in culture separates that did not undergo heating (Figure 4). Thus, nonenzymatic redox-active compounds were responsible for around 37% of the total activity that reduced ferric to ferrous iron in *M. barkeri* cultures. This is consistent with a previous report, which measured 11% of this activity in unfiltered heat-treated cultures 14 days after the addition of ferrihydrite.¹⁷ The heat treatment did not prevent ZVI from forming. The peaks of Fe(0) appeared in the XRD spectra from both heat-treated separates 30 min after the addition of ferrihydrite (SI Figure S12). These peaks disappeared after 28 days in the presence of heat-treated *M. barkeri* cells (in organic-free medium), but were still detectable after 42 days in heat-treated spent supernatants. Given that ZVI was not detected in 42-day-old spent supernatants that did not undergo any heat treatment, the heat treatment appeared to have increased the persistence of ZVI in organic-containing medium.

4. DISCUSSION

Various microorganisms, including *M. barkeri*, have been shown to reduce iron oxides and mediate the formation of different Fe(II)-containing minerals.^{6–11,17,18} This work provides the first evidence that archaea can mediate the rapid precipitation of ZVI in the presence of Fe(III). The precipitation of Fe(0) requires the presence of soluble, redox-active compounds that can interact with ferric iron and stabilize ZVI and can occur in the absence of cells and enzymatic activity. At 37 °C, this reduced phase was stabilized over periods longer than one month only in the presence of both *M. barkeri* cells and soluble organic compounds.

The mechanism of electron transport during the formation of Fe(0) remains to be elucidated. The detection of ZVI in spent supernatants and the lack of spatial associations among *M. barkeri* cells and ferrihydrite, titanomagnetite and ZVI support the extracellular reduction of ferrihydrite to Fe(II) and ZVI. Previous studies have proposed several mechanisms of extracellular electron transport between microbes and minerals: (1) electrically conductive pili or nanowires, (2) chelating compounds that reduce and solubilize Fe(III) minerals, and (3) soluble electron carriers.^{2,17} We did not observe any pili or nanowires by SEM, so the last two mechanisms are more likely to occur under our experimental conditions.

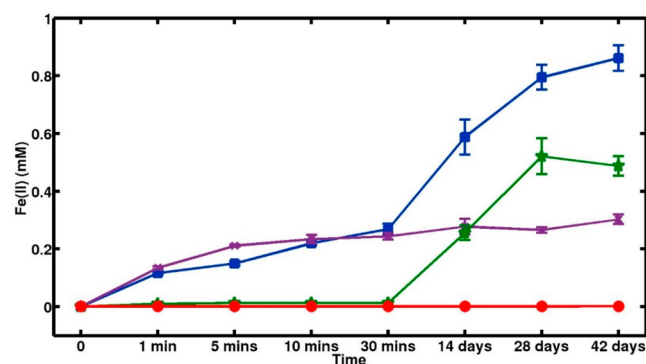


Figure 4. Change of Fe(II) concentration in organic-free medium with cells (purple line and crosses), filter-sterilized spent supernatants (green line and stars), sterile control (red line and circles) and procedure control that contained recombined filtered cells and spent supernatants (blue line and squares). Each point shows the average concentration from triplicate bottles and the error bars show the standard deviation.

M. barkeri synthesizes several electron carriers with low redox potentials, including ferredoxin, coenzyme F420, coenzyme B and methanophenazine (Table 2).¹⁵ According to the Eh–pH diagram for the Fe–CO₂–H₂O system,^{45,46} ZVI can be stable in the Eh range from about –450 mV to –650 mV at pH values 5–7 seen in our carbonate-buffered system. This is comparable to the redox potential of ferredoxin (–500 mV) (Table 2), although the roles of this and other carriers remain to be tested. As stated previously, enzymatic activity cannot account for the rapid formation of ZVI by the heat-treated *M. barkeri* cells and spent supernatants. Furthermore, due to the poor solubility of methanophenazine in water and its strong association with cell membranes,⁴⁷ we suspect that this compound is not critical for the formation of ZVI in spent supernatants or at a distance from *M. barkeri* cells.

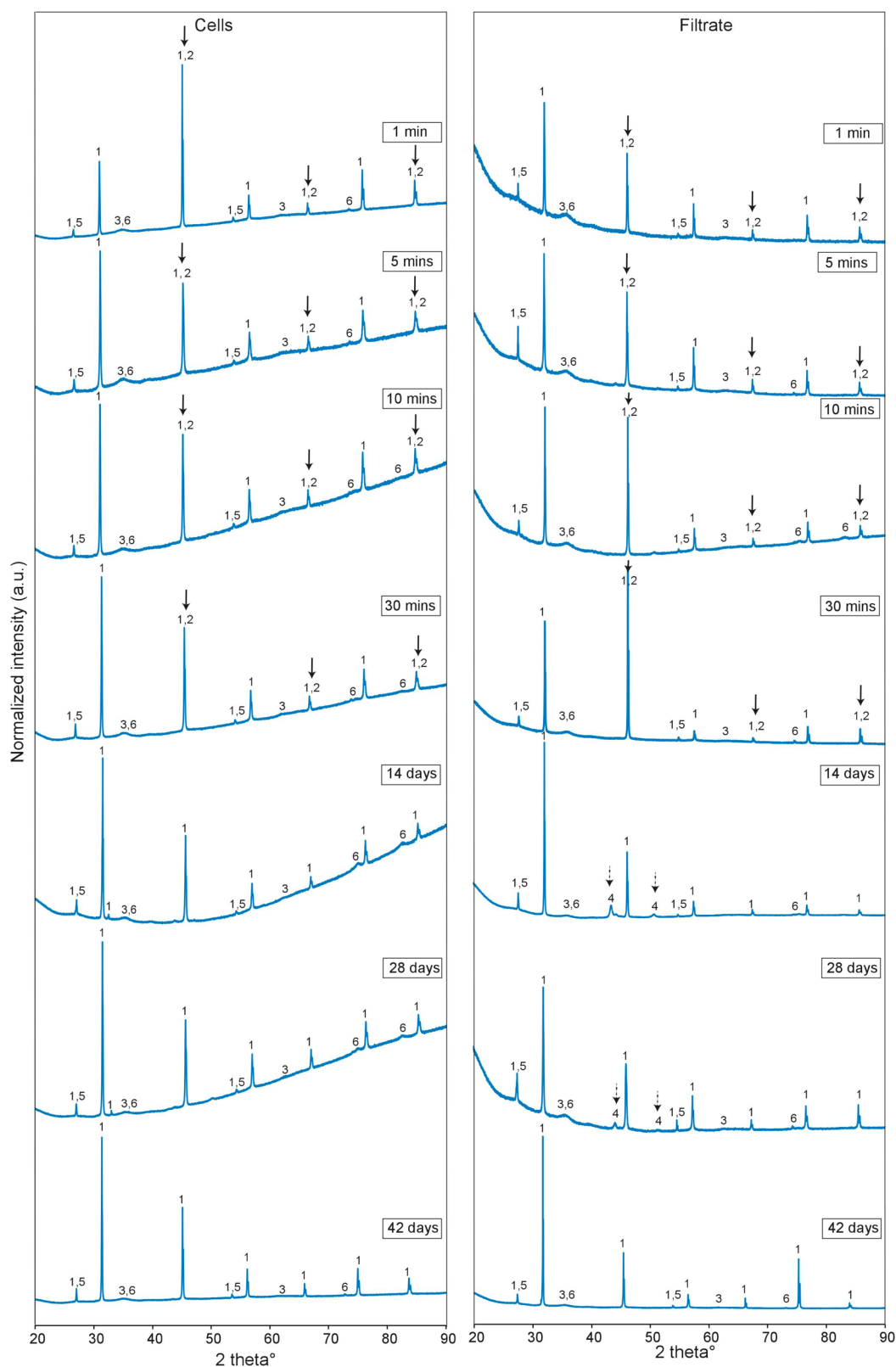


Figure 5. XRD spectra of minerals sampled from serum bottles that contained cells in organic-free medium (left column) and filter-sterilized spent supernatants (right column). The medium was reduced by Ti(III)-citrate, and the headspace gas was replaced by N_2/CO_2 before the addition of ferrihydrite. The solids were sampled at 1, 5, and 10 min, 30 min, 14 days, 28 days, and 42 days after the addition of ferrihydrite. XRD peak assignments: (1) Halite ($NaCl$); (2) Ferrite [$\alpha-Fe(0)$]; (3) Ferrihydrite (Fe_2O_3); (4) Austenite [$\gamma-Fe(0)$]; (5) Rutile (TiO_2); and (6) Titanomagnetite ($Ti_2Fe_3O_4$).

Our experimental results do not directly link the formation of ZVI to the interactions between cellular metabolism and Fe

cations. In fact, our observations suggest that *M. barkeri* cells and/or any cell-associated surface organics that are not

removed during the washing procedure and/or the heat treatment can promote the formation of ZVI and that active metabolism is not essential. Potential electron donors for the reduction of ferric iron to ZVI in *M. barkeri* cultures include membrane-associated or water-soluble redox-active compounds such as enzymes, coenzymes, or even amino acids such as L-cysteine. Although the tentative appearance of ZVI in a few organic-amended sterile controls suggested that the organic additives (yeast extract and casitone) might promote the production of ZVI, they were not effective at stabilizing it under our experimental conditions. Given that Fe(0) formed in the heat-treated organic-free cell cultures and heat-treated spent supernatants, a major contribution of heat-destabilized enzymes is also unlikely. Instead, the formation of ZVI depends primarily on nonenzymatic and soluble metabolites produced by *M. barkeri* in organic-replete media.

The long-term persistence of ZVI in *M. barkeri* cultures requires soluble organic compounds. In keeping with this,

Table 2. Relevant Redox Half-Reactions at pH = 7

possible redox half reaction	E° (mV)
Ferredoxin (ox) \rightarrow Ferredoxin (red)	-500 [ref 15]
Coenzyme F ₄₂₀ (ox) \rightarrow Coenzyme F ₄₂₀	-360 [ref 15]
Coenzyme B (ox) \rightarrow Coenzyme B (red)	-140 [ref 15]
Methanophenazine (ox) \rightarrow Methanophenazine (red)	-165 [ref 15]
Fe(III) \rightarrow Fe(0)	-37 [ref 22]

Fe(0) peaks persist longer in the XRD spectra of spent supernatants compared to those of the cells incubated in the organic-free medium (Figure 5). The metabolite(s) produced by *M. barkeri* may be similar to the ZVI-stabilizing L-cysteine.⁴¹ Previous attempts to synthesize ZVI in an ecologically friendly manner have produced Fe(0) by adding Fe(III) as FeNO₃ or FeCl₃ to plant extracts.^{32,33} The formation of ZVI in the presence of polyphenols from plant extracts contributed to the blackening of solutions^{32,33} in a manner similar to that shown in [Figure 1(b)]. The E° of these compounds range from 300 mV to 800 mV,^{32,33} which is higher compared to the potentials in *M. barkeri* cultures. It is unclear whether the cultures of *M. barkeri* contain phenolic compounds, but we speculate that the low redox potential in the methanogen cultures (Table 2) further facilitates the reduction of iron from ferric to metallic state and the stabilization of ZVI.

5. ENVIRONMENTAL IMPLICATIONS

Microbially mediated iron corrosion is a known natural process and a major industrial and engineering concern.^{48–50} Methanogenic archaea, sulfate reducing bacteria, acetogenic bacteria and nitrate reducing bacteria are all able to oxidize Fe(0) under anaerobic conditions.⁵⁰ Our results demonstrate that *M. barkeri* can mediate the reverse process, wherein Fe(III) in ferrihydrite is reduced and stabilized as ZVI. This expands the list of microbially mediated iron reduction reactions and biomineralization processes. In light of our results, ZVI may form and become stabilized in reducing and organic-rich anaerobic environments. If ZVI produced in this manner can interact with other elemental cycles, then it can be readily oxidized to Fe(II)/Fe(III) and therefore not detectable.

Biogenic magnetite is widespread in marine^{51,52} and riverine sediments.^{19,53} This mineral can be produced by different microorganisms including bacteria (e.g., magnetotactic bacteria,^{51,52} *Geobacter*^{54,55} and *Shewanella*⁵⁶), archaea (e.g.,

*Methanosarcinaceae*¹⁹), and fungi (e.g., *Fusarium oxysporum* and *Verticillium sp.*⁵⁷). Recent studies have shown that electrically conductive substances such as magnetite, hematite, and graphite facilitate direct interspecies electron transfer (DIET)^{19,54} and promote syntrophic cooperation in microbial communities.^{58–60} For example, magnetite can enhance the electron transfer from *G. sulfurreducens* to *T. denitrificans* and facilitate nitrate reduction by *T. denitrificans*.⁵⁸ Magnetic minerals in deep sediments carry paleomagnetic information that can be altered by phase transformations during diagenesis.^{61,62} Magnetite and ZVI produced by anaerobic microorganisms such as methanogens are examples of phases that can influence the paleomagnetic records. Ferrihydrite is ubiquitous in nature;⁴⁰ its delivery to reducing and organic-rich anaerobic environments may enable microbial precipitation of ZVI (i.e., a conductive and reactive material) that then promotes DIET in the communities of anaerobes.^{63,64} Fe(0) peaks were not reported in the XRD spectra in the studies of DIET in the presence of microbial iron reduction.^{19,55–57} Their absence might indicate that the redox conditions or organic compounds in these studies did not support the formation and/or stabilization of ZVI or that the produced ZVI was oxidized during the processes of mineral characterization. Our experiments tested for Fe(0) production by *M. barkeri* only, so it remains to be seen whether ZVI formation by methanogens is a ubiquitous phenomenon.

The impact of exogenously added ZVI on the structure of microbial communities in aquifer sediments⁶⁵ and soils⁶⁶ is an area of active research. For example, several studies of pure cultures have reported that ZVIs are toxic to *Escherichia coli*,^{67,68} *Dehalococcoides* spp.,⁶⁹ and *Desulfosporosinus* spp.^{65,70} Thus, ZVI particles produced naturally by *M. barkeri* or other methanogens may influence the ecology of anaerobic environments by inhibiting the growth of some microbes and promoting the growth of Fe(0)-resistant anaerobes (e.g., *Raoultella planticola*⁷¹ and *Alcaligenes eutrophus*⁷²). Previous studies have shown that the reduction of ferric to ferrous iron by methanogens can compete with methanogenesis.^{17,18} Any ZVI particles produced by methanogenic archaea might also intersect with the biogeochemical cycles of carbon and sulfur by either enhancing^{73,74} or inhibiting⁷⁵ methanogenesis and inhibiting biological sulfate reduction.^{65,70} These results imply that the production of Fe(0) by methanogens may affect both the reduction of CO₂ and the accumulation of CH₄ in anaerobic environments and CH₄-consuming microbes. In our experiments and other studies,^{17,18} methanogenesis was inhibited after the addition of ferrihydrite into the *M. barkeri* cultures. However, the main goal of our experiments was to characterize minerals in pure cultures of iron-reducing *M. barkeri* as a function of the cellular and enzymatic activity. Further experiments are needed to determine the impact of ZVI formation on both methanogenesis and the anaerobic oxidation of CH₄ in natural communities.

The microbially mediated production of ZVI may find industrial applications in metal protection and green synthesis. Microorganisms can inhibit iron corrosion by several indirect mechanisms, such as the formation of protective films and consumption of corrosive substances.^{47,76} The reverse iron corrosion in *M. barkeri* cultures shows that at least this microbe can form and stabilize ZVI in anaerobic and organic-rich environments that receive labile forms of ferric iron such as ferrihydrite. These conditions can be explored further to identify the range of chemical conditions and more complex

microbial communities that protect steel. Given that microbial methanogenesis is widespread in various terrestrial or marine environments and industrial or water-treatment facilities,^{77–80} the availability of methanogenic enrichments and organic-rich fluids from these systems should be conducive to cost-effective green synthesis of ZVI.

■ ASSOCIATED CONTENT

SI Supporting Information

The Supporting Information is available free of charge at <https://pubs.acs.org/doi/10.1021/acs.est.0c01595>.

Medium recipe; X-ray diffraction (XRD) spectra under different experimental conditions; Rietveld analyses of XRD spectra; microfocused X-ray diffraction; X-ray photoelectron spectroscopy; thermomagnetic measurements; scanning electron microscope images; and Fe(II) concentration measurements (PDF)

■ AUTHOR INFORMATION

Corresponding Author

Haitao Shang – Department of Earth, Atmospheric and Planetary Sciences, Massachusetts Institute of Technology, Cambridge, Massachusetts 02139, United States; orcid.org/0000-0002-5731-4559; Email: hts@mit.edu

Authors

Mirna Daye – Department of Earth, Atmospheric and Planetary Sciences, Massachusetts Institute of Technology, Cambridge, Massachusetts 02139, United States

Orit Sivan – Department of Geological and Environmental Sciences, Ben Gurion University of the Negev, Beer Sheva 84105, Israel; orcid.org/0000-0002-0796-2291

Caue S. Borlina – Department of Earth, Atmospheric and Planetary Sciences, Massachusetts Institute of Technology, Cambridge, Massachusetts 02139, United States

Nobumichi Tamura – Advanced Light Source, Lawrence Berkeley National Laboratory, Berkeley, California 94720, United States

Benjamin P. Weiss – Department of Earth, Atmospheric and Planetary Sciences, Massachusetts Institute of Technology, Cambridge, Massachusetts 02139, United States

Tanja Bosak – Department of Earth, Atmospheric and Planetary Sciences, Massachusetts Institute of Technology, Cambridge, Massachusetts 02139, United States

Complete contact information is available at: <https://pubs.acs.org/doi/10.1021/acs.est.0c01595>

Notes

The authors declare no competing financial interest.

■ ACKNOWLEDGMENTS

We thank the current members of the Bosak laboratory, the Simons Foundation Collaboration on the Origins of Life grants no. 327126 to T.B., NSF FESD grant no. 14-374 to T.B., and the MIT-Israel program award no. 2629055 to T.B. and O.S. The NSF award number DMR-1419807 funded MIT Center for Material Science and Engineering (part of Materials Research Science and Engineering Center, NSF ECCS award no. 1541959) and funded the Harvard University Center for Nanoscale Systems (CNS), a member of the National Nanotechnology Coordinated Infrastructure Network (NNCI). The DOE Office of Science User Facility under

contract no. DE-AC02-05CH11231 supports the Advanced Light Source and BI L12.3.2.

■ REFERENCES

- (1) Weber, K. A.; Achenbach, L. A.; Coates, J. D. Microorganisms pumping iron: anaerobic microbial iron oxidation and reduction. *Nat. Rev. Microbiol.* **2006**, *4*, 752–764.
- (2) Melton, E. D.; Swanner, E. D.; Behrens, S.; Schmidt, C.; Kappler, D. The interplay of microbially mediated and abiotic reactions in the biogeochemical Fe cycle. *Nat. Rev. Microbiol.* **2014**, *12*, 797–808.
- (3) Konhauser, K. O.; Kappler, A.; Roden, E. E. Iron in microbial metabolisms. *Elements* **2011**, *7*, 89–93.
- (4) Fredrickson, J. K.; Gorby, Y. A. Environmental processes mediated by iron-reducing bacteria. *Curr. Opin. Biotechnol.* **1996**, *7*, 287–294.
- (5) Luu, Y. S.; Ramsay, J. A. Review: Microbial mechanisms of accessing insoluble Fe(III) as an energy source. *World J. Microbiol. Biotechnol.* **2003**, *19*, 215–225.
- (6) Lovley, D. R.; Stolz, J. F.; Nord, G. L.; Phillips, E. J. P. Anaerobic production of magnetite by a dissimilatory iron-reducing microorganism. *Nature* **1987**, *330*, 252–254.
- (7) Bell, P. E.; Mills, A. L.; Herman, J. S. Biogeochemical conditions favoring magnetite formation during anaerobic iron reduction. *Appl. Environ. Microbiol.* **1987**, *53*, 2610–2616.
- (8) Liu, D.; Wang, H.; Dong, H.; Qiu, X.; Dong, X.; Cravotta, C. A., III Mineral transformations associated with goethite reduction by *Methanosarcina barkeri*. *Chem. Geol.* **2011**, *288*, 53–60.
- (9) Dong, H.; Kostka, J. E.; Kim, J. Microscopic evidence for microbial dissolution of smectite. *Clays Clay Miner.* **2003**, *51*, 502–512.
- (10) Kim, J.; Dong, H.; Seabaugh, J.; Newell, S. W.; Eberl, D. D. Role of microbes in the smectite-to-illite reaction. *Science* **2004**, *303*, 830–832.
- (11) Roh, Y.; Zhang, C. L.; Vali, H.; Lauf, R. J.; Zhou, J.; Phelps, T. J. Biogeochemical and environmental factors in Fe biomineralization: magnetite and siderite formation. *Clays Clay Miner.* **2003**, *51*, 83–95.
- (12) Ferry, J. G. *Methanogenesis: Ecology, Physiology, Biochemistry & Genetics*; Springer-Verlag: New York, NY, 2012.
- (13) Jones, W. J.; Nagle, D. P., Jr; Whitman, W. B. Methanogens and the diversity of archaeobacteria. *Microbiol. Rev.* **1987**, *51*, 135–177.
- (14) Fetzter, S.; Conrad, R. Effect of redox potential on methanogenesis by *Methanosarcina barkeri*. *Arch. Microbiol.* **1993**, *160*, 108–113.
- (15) Thauer, R. K.; Kaster, A. K.; Seedorf, H.; Buckel, W.; Hedderich, R. Methanogenic archaea: ecologically relevant differences in energy conservation. *Nat. Rev. Microbiol.* **2008**, *6*, 579–591.
- (16) Wiedemeier, T. H.; Rifai, H. S.; Newell, C. J.; Wilson, J. T. *Natural Attenuation of Fuels and Chlorinated Solvents in the Subsurface*; John Wiley & Sons: New York, 1999.
- (17) Sivan, O.; Shusta, S. S.; Valentine, D. Methanogens rapidly transition from methane production to iron reduction. *Geobiology* **2016**, *14*, 190–203.
- (18) Bodegom, P. M.; Scholten, J. C.M.; Stams, A. J.M. Direct inhibition of methanogenesis by ferric iron. *FEMS Microbiol. Ecol.* **2004**, *49*, 261–268.
- (19) Zheng, S.; Wang, B.; Liu, F.; Wang, O. Magnetite production and transformation in the methanogenic consortia from coastal riverine sediments. *J. Microbiol.* **2017**, *55*, 862–870.
- (20) Liu, D.; Dong, H.; Bishop, M. E.; Wang, H.; Agrawal, A.; Tritschler, S.; Eberl, D. D.; Xie, S. Reduction of structural Fe(III) in nontronite by methanogen *Methanosarcina barkeri*. *Geochim. Cosmochim. Acta* **2011**, *75*, 1057–1071.
- (21) Bond, D. R.; Lovley, D. R. Reduction of Fe(III) oxide by methanogens in the presence and absence of extracellular quinones. *Environ. Microbiol.* **2002**, *4*, 115–124.
- (22) Vanysek, P. *Electrochemical Series*; CRC Press: Boca Raton, FL, 2000.

- (23) Revie, W. R. *Corrosion and Corrosion Control: An Introduction to Corrosion Science and Engineering*; John Wiley & Sons: Hoboken, NJ, 2008.
- (24) Enning, D.; Garrelfs, J. Corrosion of iron by sulfate-reducing bacteria - new views of an old problem. *Appl. Environ. Microbiol.* **2014**, *80*, 1226–1236.
- (25) Dinh, H. T.; Kuever, J.; Mußmann, M.; Hassel, A. W.; Stratmann, M.; Widdel, F. Iron corrosion by novel anaerobic microorganisms. *Nature* **2004**, *427*, 829–832.
- (26) Daniels, L.; Belay, N.; Rajagopal, B. S.; Weimer, P. J. Bacterial methanogenesis and growth from CO₂ with elemental iron as the sole source of electrons. *Science* **1987**, *237*, 509–511.
- (27) Lee, W.; Characklis, W. G. Corrosion of mild steel under anaerobic biofilm. *Corrosion* **1993**, *49*, 186–199.
- (28) Pineau, A.; Kanari, N.; Gaballah, I. Kinetics of reduction of iron oxides by H₂: Part I: low temperature reduction of hematite. *Thermochim. Acta* **2006**, *447*, 89–100.
- (29) Pineau, A.; Kanari, N.; Gaballah, I. Kinetics of reduction of iron oxides by H₂: Part II: low temperature reduction of magnetite. *Thermochim. Acta* **2007**, *456*, 75–88.
- (30) Chen, Y.; Chen, S.; Chen, Q.; Zhou, Z.; Sun, S. Electrochemical preparation of iron cuboid nanoparticles and their catalytic properties for nitrite reduction. *Electrochim. Acta* **2008**, *53*, 6938–6943.
- (31) Klein, F.; Bach, W. Fe-Ni-Co-O-S phase relations in peridotite–seawater interactions. *J. Petrol.* **2009**, *50*, 37–59.
- (32) Hoag, G. E.; Collins, J. B.; Holcomb, J. L.; Hoag, J. R.; Nadagouda, M. M.; Varma, R. S. Degradation of bromothymol blue by greener nano-scale zero-valent iron synthesized using tea polyphenols. *J. Mater. Chem.* **2009**, *19*, 8671–8677.
- (33) Nadagouda, M. N.; Castle, A. B.; Murdock, R. C.; Hussain, S. M.; Varma, R. S. In vitro biocompatibility of nanoscale zero-valent iron particles (NZVI) synthesized using tea polyphenols. *Green Chem.* **2010**, *12*, 114–122.
- (34) Machado, S.; Pinto, S. L.; Grosso, J. P.; Nouws, H. P. A.; Albergaria, J. T.; Delerue-Matos, C. Green production of zero-valent iron nanoparticles using tree leaf extracts. *Sci. Total Environ.* **2013**, *445*, 1–8.
- (35) Rahman, P. K. S. M.; Bastola, S. Biological reduction of iron to the elemental state from ochre deposits of Skelton beck in northeast England. *Front. Environ. Sci.* **2014**, *2* (22), 1–8.
- (36) Wolfe, R. S.; Metcalf, W. W. A vacuum-vortex technique for preparation of anoxic solutions or liquid culture media in small volumes for cultivating methanogens or other strict anaerobes. *Anaerobe* **2010**, *16*, 216–219.
- (37) Viollier, E.; Inglett, P. W.; Hunter, K. S.; Roychoudhury, A. N.; Van Cappellen, P. The ferrozine method revisited: Fe(II)/Fe(III) determination in natural waters. *Appl. Geochem.* **2000**, *15*, 785–790.
- (38) Rietveld, H. M. A profile refinement method for nuclear and magnetic structures. *J. Appl. Crystallogr.* **1969**, *2*, 65–71.
- (39) Garrick-Bethell, I.; Weiss, B. P. Kamacite blocking temperatures and applications to lunar magnetism. *Earth Planet. Sci. Lett.* **2010**, *294*, 1–7.
- (40) Jambor, J. L.; Dutrizac, J. E. Occurrence and constitution of natural and synthetic ferrihydrite, a widespread iron oxyhydroxide. *Chem. Rev.* **1998**, *98*, 2549–2586.
- (41) Bagbi, Y.; Sarswat, A.; Tiwari, S.; Mohan, D.; Pandey, A.; Solanki, P. R. Synthesis of L-cysteine stabilized zero-valent iron (NZVI) nanoparticles for lead remediation from water. *Environmental Nanotechnology, Monitoring & Management* **2017**, *7*, 34–45.
- (42) Zachara, J. M.; Kukkadapu, R. K.; Fredrickson, J. K.; Gorby, Y. A.; Smith, S. C. Biomineralization of poorly crystalline Fe(III) oxides by dissimilatory metal reducing bacteria (DMRB). *Geomicrobiol. J.* **2002**, *19*, 179–207.
- (43) Tosca, N. J.; Ahmed, I. A. M.; Tutolo, B. M.; Ashpittel, A.; Hurowitz, J. A. Magnetite authigenesis and the warming of early mars. *Nat. Geosci.* **2018**, *11*, 635–639.
- (44) Usman, M.; Byrne, J. M.; Chaudhary, A.; Orsetti, S.; Hanna, K.; Ruby, C.; Kappler, A.; Haderlein, S. B. Magnetite and green rust: synthesis, properties, and environmental applications of mixed-valent iron minerals. *Chem. Rev.* **2018**, *118*, 3251–3304.
- (45) Azoulay, I.; Rémaizeilles, C.; Refait, P. Determination of standard Gibbs free energy of formation of chukanovite and Pourbaix diagrams of iron in carbonated media. *Corros. Sci.* **2012**, *58*, 229–236.
- (46) Drissi, S. H.; Refait, P.; Abdelmoula, M.; Génin, J. M. R. The preparation and thermodynamic properties of Fe(II)–Fe(III) hydroxide-carbonate (green rust 1); Pourbaix diagram of iron in carbonate-containing aqueous media. *Corros. Sci.* **1995**, *37* (12), 2025–2041.
- (47) Abken, H. J.; Tietze, M.; Brodersen, J.; Bäumer, S.; Beifuss, U.; Deppenmeier, U. Isolation and characterization of methanophenazine and function of phenazines in membrane-bound electron transport of *Methanosarcina Mazei* Gol. *J. Bacteriol.* **1998**, *180*, 2027–2032.
- (48) Kip, N.; van Veen, J. A. The dual role of microbes in corrosion. *ISME J.* **2015**, *9*, 542–551.
- (49) Videla, H. A.; Herrera, L. K. Microbiologically influenced corrosion: looking to the future. *Int. Microbiol.* **2005**, *8*, 169–180.
- (50) Kato, S. Microbial extracellular electron transfer and its relevance to iron corrosion. *Microb. Biotechnol.* **2016**, *9*, 141–148.
- (51) Bazylynski, D. A.; Frankel, R. B.; Jannasch, H. W. Anaerobic magnetite production by a marine, magnetotactic bacterium. *Nature* **1988**, *334*, 518–519.
- (52) Stolz, J. F.; Chang, S. R.; Kirschvink, J. L. Magnetotactic bacteria and single-domain magnetite in hemipelagic sediments. *Nature* **1986**, *321*, 849–851.
- (53) Lovley, D. R.; Phillips, E. J. P. Availability of ferric iron for microbial reduction in bottom sediments of the freshwater tidal Potomac River. *Appl. Environ. Microbiol.* **1986**, *52*, 751–757.
- (54) Tang, J.; Zhuang, L.; Ma, J.; Tang, Z.; Yu, Z.; Zhou, S. Secondary mineralization of ferrihydrite affects microbial methanogenesis in *Geobacter-Methanosarcina* cocultures. *Appl. Environ. Microbiol.* **2016**, *82*, 5869–5877.
- (55) Coker, V. S.; Bell, A. M. T.; Pearce, C. I.; Patrick, R. A. D.; van der Laan, G.; Lloyd, J. R. Time-resolved synchrotron powder X-ray diffraction study of magnetite formation by the Fe(III)-reducing bacterium *Geobacter sulfurreducens*. *Am. Mineral.* **2008**, *93*, 540–547.
- (56) Roh, Y.; Gao, H.; Vali, H.; Kennedy, D. W.; Yang, Z. K.; Gao, W.; Dohnalkova, A. C.; Stapleton, R. D.; Moon, J. W.; Phelps, T. J.; Fredrickson, J. K.; Zhou, J. Metal reduction and iron biomineralization by a psychrotolerant Fe(III)-reducing bacterium, *Shewanella* sp. strain PV-4. *Appl. Environ. Microbiol.* **2006**, *72*, 3236–3244.
- (57) Bharde, A.; Rautaray, D.; Bansal, V.; Ahmad, A.; Sarkar, I.; Yusuf, S. M.; Sanyal, M.; Sastry, M. Extracellular biosynthesis of magnetite using fungi. *Small* **2006**, *2*, 135–141.
- (58) Kato, S.; Hashimoto, K.; Watanabe, K. Microbial interspecies electron transfer via electric currents through conductive minerals. *Proc. Natl. Acad. Sci. U. S. A.* **2012**, *109*, 10042–10046.
- (59) Aulenta, F.; Rossetti, S.; Amalfitano, S.; Majone, M.; Tandoi, V. Conductive magnetite nanoparticles accelerate the microbial reductive dechlorination of trichloroethene by promoting interspecies electron transfer processes. *ChemSusChem* **2013**, *6*, 433–436.
- (60) Kouzuma, A.; Kato, S.; Watanabe, K. Microbial interspecies interactions: recent findings in syntrophic consortia. *Front. Microbiol.* **2015**, *6* (477), 1–8.
- (61) Kasten, S.; Freudenthal, T.; Gingele, F. X.; Schulz, H. D. Simultaneous formation of iron-rich layers at different redox boundaries in sediments of the Amazon deep-sea fan. *Geochim. Cosmochim. Acta* **1998**, *62*, 2253–2264.
- (62) Riedinger, N.; Pfeifer, K.; Kasten, S.; Garming, J. F. L.; Vogt, C.; Hensen, C. Diagenetic alteration of magnetic signals by anaerobic oxidation of methane related to a change in sedimentation rate. *Geochim. Cosmochim. Acta* **2005**, *69*, 4117–4126.
- (63) Lefevre, E.; Bossa, N.; Wiesner, M. R.; Gunsch, C. K. A review of the environmental implications of in situ remediation by nanoscale zero-valent iron (nZVI): behavior, transport and impacts on microbial communities. *Sci. Total Environ.* **2016**, *565*, 889–901.
- (64) Xie, Y.; Dong, H.; Zeng, G.; Tang, L.; Jiang, Z.; Zhang, C.; Deng, J.; Zhang, L.; Zhang, Y. The interactions between nanoscale

zero-valent iron and microbes in the subsurface environment: a review. *J. Hazard. Mater.* **2017**, *321*, 390–407.

(65) Kumar, N.; Omoregie, E. O.; Rose, J.; Masion, A.; Lloyd, J. R.; Diels, L.; Bastiaens, L. Inhibition of sulfate reducing bacteria in aquifer sediment by iron nanoparticles. *Water Res.* **2014**, *51*, 64–72.

(66) Tilston, E. L.; Collins, C. D.; Mitchell, G. R.; Princivalle, J.; Shaw, L. J. Nanoscale zerovalent iron alters soil bacterial community structure and inhibits chloroaromatic biodegradation potential in Aroclor 1242-contaminated soil. *Environ. Pollut.* **2013**, *173*, 38–46.

(67) Auffan, M.; Achouak, W.; Rose, J.; Roncato, M. A.; Chaneac, C.; Waite, D. T.; Masion, A.; Woicik, J. C.; Wiesner, M. R.; Bottero, J. Y. Relation between the redox state of iron-based nanoparticles and their cytotoxicity toward *Escherichia coli*. *Environ. Sci. Technol.* **2008**, *42*, 6730–6735.

(68) Lee, C.; Kim, J. Y.; Lee, W. I.; Nelson, K. L.; Yoon, J.; Sedlak, D. L. Bactericidal effect of zero-valent iron nanoparticles on *Escherichia coli*. *Environ. Sci. Technol.* **2008**, *42*, 4927–4933.

(69) Xiu, Z.; Jin, Z.; Li, T.; Mahendra, S.; Lowry, G. V.; Alvarez, P. J. Effects of nano-scale zero-valent iron particles on a mixed culture dechlorinating trichloroethylene. *Bioresour. Technol.* **2010**, *101*, 1141–1146.

(70) Barnes, R. J.; Riba, O.; Gardner, M. N.; Singer, A. C.; Jackman, S. A.; Thompson, I. P. Inhibition of biological TCE and sulphate reduction in the presence of iron nanoparticles. *Chemosphere* **2010**, *80*, 554–562.

(71) Fajardo, C.; Ortiz, L. T.; Rodriguez-Membibre, M. L.; Nande, M.; Lobo, M. C.; Martin, M. Assessing the impact of zero-valent iron (ZVI) nanotechnology on soil microbial structure and functionality: a molecular approach. *Chemosphere* **2012**, *86*, 802–808.

(72) An, Y.; Li, T.; Jin, Z.; Dong, M.; Li, Q.; Wang, S. Decreasing ammonium generation using hydrogenotrophic bacteria in the process of nitrate reduction by nanoscale zero-valent iron. *Sci. Total Environ.* **2009**, *407*, 5465–5470.

(73) Carpenter, A. W.; Laughton, S. N.; Wiesner, M. R. Enhanced biogas production from nanoscale zero valent iron-amended anaerobic bioreactors. *Environ. Eng. Sci.* **2015**, *32*, 647–655.

(74) Su, C.; Puls, R. W.; Krug, T. A.; Watling, M. T.; O'Hara, S. K.; Quinn, J. W.; Ruiz, N. E. Travel distance and transformation of injected emulsified zerovalent iron nanoparticles in the subsurface during two and half years. *Water Res.* **2013**, *47*, 4095–4106.

(75) Yang, Y.; Guo, J.; Hu, Z. Impact of nano zero-valent iron (NZVI) on methanogenic activity and population dynamics in anaerobic digestion. *Water Res.* **2013**, *47*, 6790–6800.

(76) Dubiel, M.; Hsu, C. H.; Chien, C. C.; Mansfeld, F. B.; Newman, D. K. Microbial iron respiration can protect steel from corrosion. *Appl. Environ. Microbiol.* **2002**, *68*, 1440–1445.

(77) Serrano-Silva, N.; Sarria-Guzman, Y.; Dendooven, L.; Luna-Guido, M. Methanogenesis and methanotrophy in soil: a review. *Pedosphere* **2014**, *24*, 291–307.

(78) Ferry, J. G.; Lessner, D. J. Methanogenesis in marine sediments. *Ann. N. Y. Acad. Sci.* **2008**, *1125*, 147–157.

(79) van den Berg, L. Developments in methanogenesis from industrial waste water. *Can. J. Microbiol.* **1984**, *30* (8), 975–990.

(80) Tabatabaei, M.; Rahim, R. A.; Abdullah, N.; Wright, A. D. G.; Shirai, Y.; Sakai, K.; Sulaiman, A.; Hassan, M. A. Importance of the methanogenic archaea populations in anaerobic wastewater treatments. *Process Biochem.* **2010**, *45*, 8, 1214–1225.

Supporting Information

Formation of Zerovalent Iron in Iron-Reducing Cultures of *Methanosarcina barkeri*

Haitao Shang ^{1*}, Mirna Daye ¹, Orit Sivan ², Caue S. Borlina ¹, Nobumichi Tamura ³, Benjamin P. Weiss ¹ and Tanja Bosak ¹

¹Department of Earth, Atmospheric and Planetary Science, Massachusetts Institute of Technology, Cambridge, Massachusetts 02139, United States

²Department of Geological and Environmental Sciences, Ben Gurion University of the Negev, Beer Sheva 84105, Israel

³Advanced Light Source, Lawrence Berkeley National Laboratory, Berkeley, California 94720, United States

*Email: hts@mit.edu

Table S1: Medium recipe -----	Page S1
Table S2: Refined unit-cell parameters of the XRD spectra of <i>M.barkeri</i> cultures and sterile controls in Figure 2 using Rietveld analyses -----	Page S2 – S4
Figure S1: Micro-focused X-ray diffraction -----	Page S5
Figure S2: X-ray photoelectron spectroscopy -----	Page S6
Figure S3: XRD spectra of <i>M. barkeri</i> cultures that tested the influence of growth phase on the mineral composition after the addition of ferrihydrite -----	Page S7
Figure S4: XRD spectra of <i>M. barkeri</i> cultures and sterile controls that tested the influence of headspace gas composition on mineral composition after the addition of ferrihydrite -----	Page S8
Figure S5: XRD spectra of <i>M. barkeri</i> cultures and sterile controls that tested the influence of the content of organic additives on mineral composition after the addition of ferrihydrite -----	Page S9
Figure S6: Thermomagnetic measurement -----	Page S10
Figure S7: Morphology of <i>M. barkeri</i> before the addition of ferrihydrite -----	Page S11
Figure S8: XRD spectra of <i>M. barkeri</i> cultures and sterile controls that tested the influence of Fe(III) source on mineral composition after the addition of ferrihydrite -----	Page S12
Figure S9: XRD spectra of <i>M. barkeri</i> cultures and sterile controls -----	Page S13
Figure S10: XRD spectra of sterile controls for the cell-filtrate separation experiment ---	Page S14
Table S3: Refined unit-cell parameters of the XRD spectra of <i>M.barkeri</i> cells in organic-free medium and spent supernatants in Figure 5 using Rietveld analyses -----	Page S15 – S20
Figure S11: Fe(II) concentrations during the reduction of ferrihydrite-----	Page S21
Figure S12: XRD spectra of <i>M. barkeri</i> cells in heat-treated organic-free medium, spent supernatants and organic-free sterile controls-----	Page S22

Table S1: Medium Recipe

Ingredient	Weight or volume	Ingredient	Weight
Distilled water	1000 mL (Final volume)	ZnCl ₂	1.0 mg
Casitone	0.5 g or 2.0 g	MnCl ₂ ·4H ₂ O	1.0 mg
Yeast extract	0.5 g or 2.0 g	AlCl ₃ ·6H ₂ O	0.4 mg
Mercaptoethanesulfonic acid	0.50 g	FeSO ₄ ·7H ₂ O	1.0 mg
Ti(III)-citrate solution (see below)	10.0 mL	H ₃ BO ₃	0.1 mg
Vitamin solution (see below)	10.0 mL	CoCl ₂ ·6H ₂ O	1.5 mg
NaEDTA·2H ₂ O	5.0 mg	CuCl ₂ ·H ₂ O	0.2 mg
K ₂ HPO ₄	0.40 g	NiSO ₄ ·6H ₂ O	0.2 mg
NH ₄ Cl	1.0 g	H ₂ SeO ₃	0.1 mg
MgCl ₂ ·6H ₂ O	1.0 g	Na ₂ WO ₄ ·2H ₂ O	0.2 mg
CaCl ₂ ·2H ₂ O	0.4 g	Na ₂ MoO ₄ ·2H ₂ O	0.1 mg

Vitamin solution (DSMZ 141), filter sterilized under anaerobic conditions

Ingredient	Weight or volume	Ingredient	Weight
Distilled water	1000 mL (Final volume)	Biotin	2.0 mg
Folic acid	2.0 mg	Pyridoxine-HCl	10.0 mg
Thiamine-HCl·2H ₂ O	5.0 mg	Riboflavin	5.0 g
Nicotinic acid	5.0 mg	D-Ca-pantothenate	5.0 mg
Vitamin B ₁₂	0.1 mg	Lipoic acid	5.0 mg
p-Aminobenzoic acid	5.0 mg		

Ti(III)-citrate solution: 2 M Ti(III)-citrate solution was prepared using TiCl₃ and Na-citrate solutions, autoclaved at 120 °C for 30 mins and diluted in sterile and anaerobic nanopure water to 85 mM, 256 mM and 768 mM.

Concentration	Ti(III)-citrate (2M) volume	Distilled water volume	Total Volume
85 mM	4.25 mL	95.75 mL	100 mL
256 mM	12.8 mL	87.2 mL	100 mL
768 mM	38.4 mL	61.6 mL	100 mL

Table S2.1 Refined unit-cell parameters of the XRD spectra of *M.barkeri* cultures (Figure 2) using Rietveld analyses

	Phase	Percentage (%)	Unit cell (Å)	d-spacing (Å)	Formula
30 mins	Halite	58.7	a= 5.6440 b= 5.6440 c= 5.6440	2.8210	NaCl
	Ferrite	15.2	a= 2.8274 b= 2.8274 c= 2.8274	1.9901	α -Fe(0)
	Ferrihydrite	12.6	a= 4.8230 b= 5.0090 c= 7.1610	2.49339	Fe ₂ O ₃
	Rutile	8.3	a= 4.9530 b= 4.9530 c= 2.9590	3.24800	TiO ₂
	Titanomagnetite	5.2	a= 8.4689 b= 8.4689 c= 8.4689	2.55437	Ti ₂ Fe ₃ O ₄
28 days	Halite	30.1	a= 5.6440 b= 5.6440 c= 5.6440	2.8210	NaCl
	Ferrite	32.1	a= 2.8274 b= 2.8274 c= 2.8274	1.9901	α -Fe(0)
	Ferrihydrite	7.2	a= 4.8230 b= 5.0090 c= 7.1610	2.49339	Fe ₂ O ₃
	Austenite	18.3	a= 3.6000 b= 3.6000 c= 3.6000	2.07846	γ -Fe(0)
	Rutile	2.2	a= 4.9530 b= 4.9530 c= 2.9590	3.24800	TiO ₂
	Titanomagnetite	10.1	a= 8.4689 b= 8.4689 c= 8.4689	2.55437	Ti ₂ Fe ₃ O ₄
42 days	Halite	78.3	a= 5.6440 b= 5.6440 c= 5.6440	2.8210	NaCl
	Ferrihydrite	5.2	a= 4.8230 b= 5.0090 c= 7.1610	2.49339	Fe ₂ O ₃
	Austenite	12.3	a= 3.6000 b= 3.6000 c= 3.6000	2.07846	γ -Fe(0)
	Titanomagnetite	4.2	a= 8.4689 b= 8.4689 c= 8.4689	2.55437	Ti ₂ Fe ₃ O ₄

Table S2.2 Refined unit-cell parameters of the XRD spectra of sterile controls (Figure 2) using Rietveld analyses

	Phase	Percentage (%)	Unit cell (Å)	d-spacing (Å)	Formula
30 mins	Halite	71.2	a= 5.6440 b= 5.6440 c= 5.6440	2.8210	NaCl
	Ferrihydrite	27	a= 4.8230 b= 5.0090 c= 7.1610	2.49339	Fe ₂ O ₃
	Rutile	1.8	a= 4.9530 b= 4.9530 c= 2.9590	3.24800	TiO ₂
28 days	Halite	69.1	a= 5.6440 b= 5.6440 c= 5.6440	2.8210	NaCl
	Ferrihydrite	27.9	a= 4.8230 b= 5.0090 c= 7.1610	2.49339	Fe ₂ O ₃
	Rutile	2.2	a= 4.9530 b= 4.9530 c= 2.9590	3.24800	TiO ₂
42 days	Halite	72.5	a= 5.6440 b= 5.6440 c= 5.6440	2.8210	NaCl
	Ferrihydrite	24.1	a= 4.8230 b= 5.0090 c= 7.1610	2.49339	Fe ₂ O ₃
	Rutile	3.4	a= 4.9530 b= 4.9530 c= 2.9590	3.24800	TiO ₂

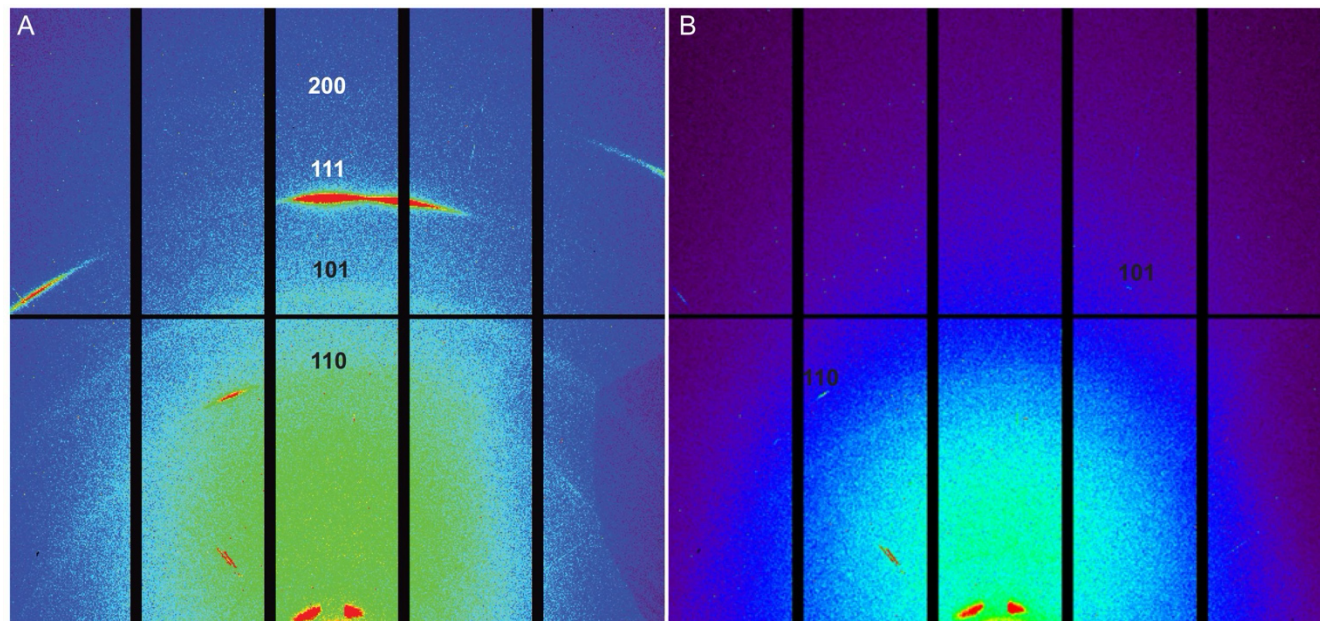


Figure S1: Diffraction pattern indices for γ -Fe(0) on the spectrum acquired by synchrotron micro-focused X-ray diffraction (μ XRD) of minerals from (A) *M. barkeri* cultures and (B) sterile control 42 days after the addition of ferrihydrite. The white lettering shows austenite [γ -Fe(0)] with 2.104 Å d-spacing. Black lettering shows halite (NaCl).

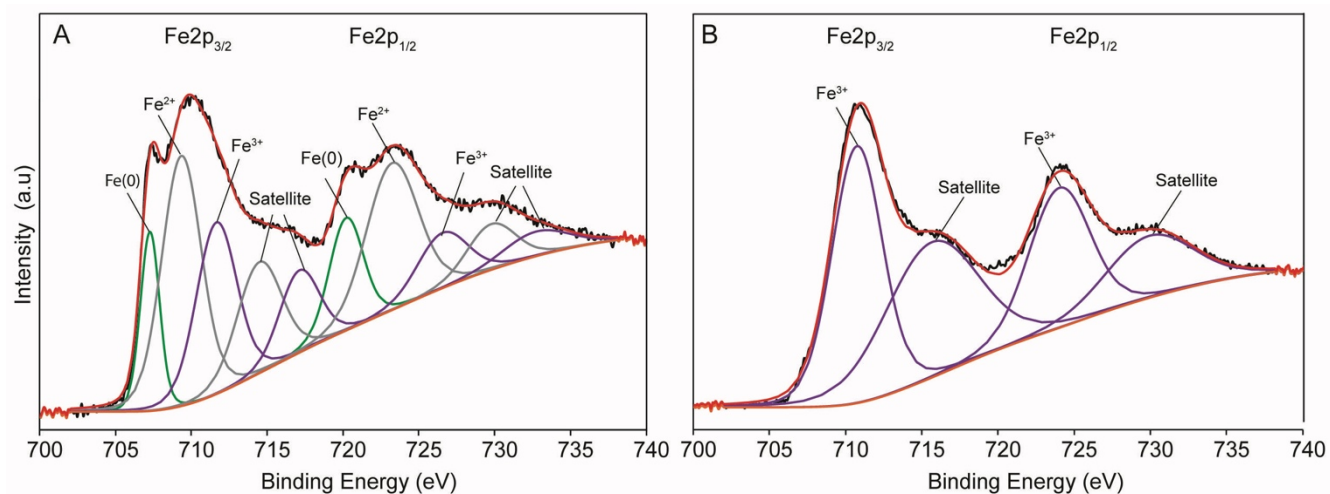


Figure S2: Redox state of iron measured by X-ray photoelectron spectroscopy (XPS) of precipitates sampled 42 days after the addition of ferrihydrite. (A) *M. barkeri* cultures. Fe(0) has two peaks at binding energies of 707.23 eV (Fe2p_{2/3}) and 720.21 eV (Fe2p_{1/2}), Fe(II) has two peaks at binding energies of 709.34 eV (Fe2p_{2/3}) and 723.13 eV (Fe2p_{1/2}), and Fe(III) has two peaks at binding energies of 711.66 eV (Fe2p_{2/3}) and 726.55 eV (Fe2p_{1/2}). (B) Sterile control. Fe(III) has two peaks at binding energies of 710.82 eV (Fe2p_{2/3}) and 724.82 (Fe2p_{1/2}). No peaks for Fe(II) or Fe(0) appeared in sterile controls.

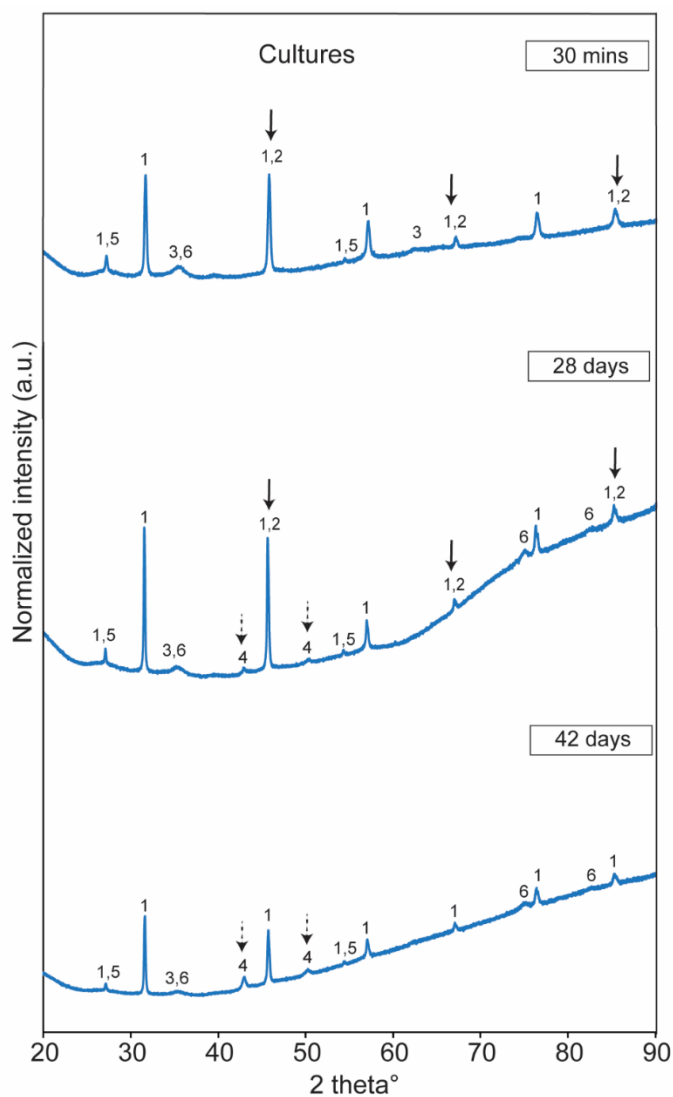


Figure S3: XRD spectra of minerals sampled from *M. barkeri* cultures in the experimental series that tested the influence of growth phase on mineral composition after the addition of ferrihydrite. The medium was reduced by Ti(III)-citrate and contained 1 g/L of organic additives and the headspace gas was replaced by N₂/CO₂ before the addition of ferrihydrite in stationary phase. The samples were collected at 30 mins, 28 days and 42 days after the addition of ferrihydrite. XRD peak assignments: (1) Halite (NaCl); (2) Ferrite [α -Fe(0)]; (3) Ferrihydrite (Fe₂O₃); (4) Austenite [γ -Fe(0)]; (5) Rutile (TiO₂); and (6) Titanomagnetite (Ti₂Fe₃O₄).

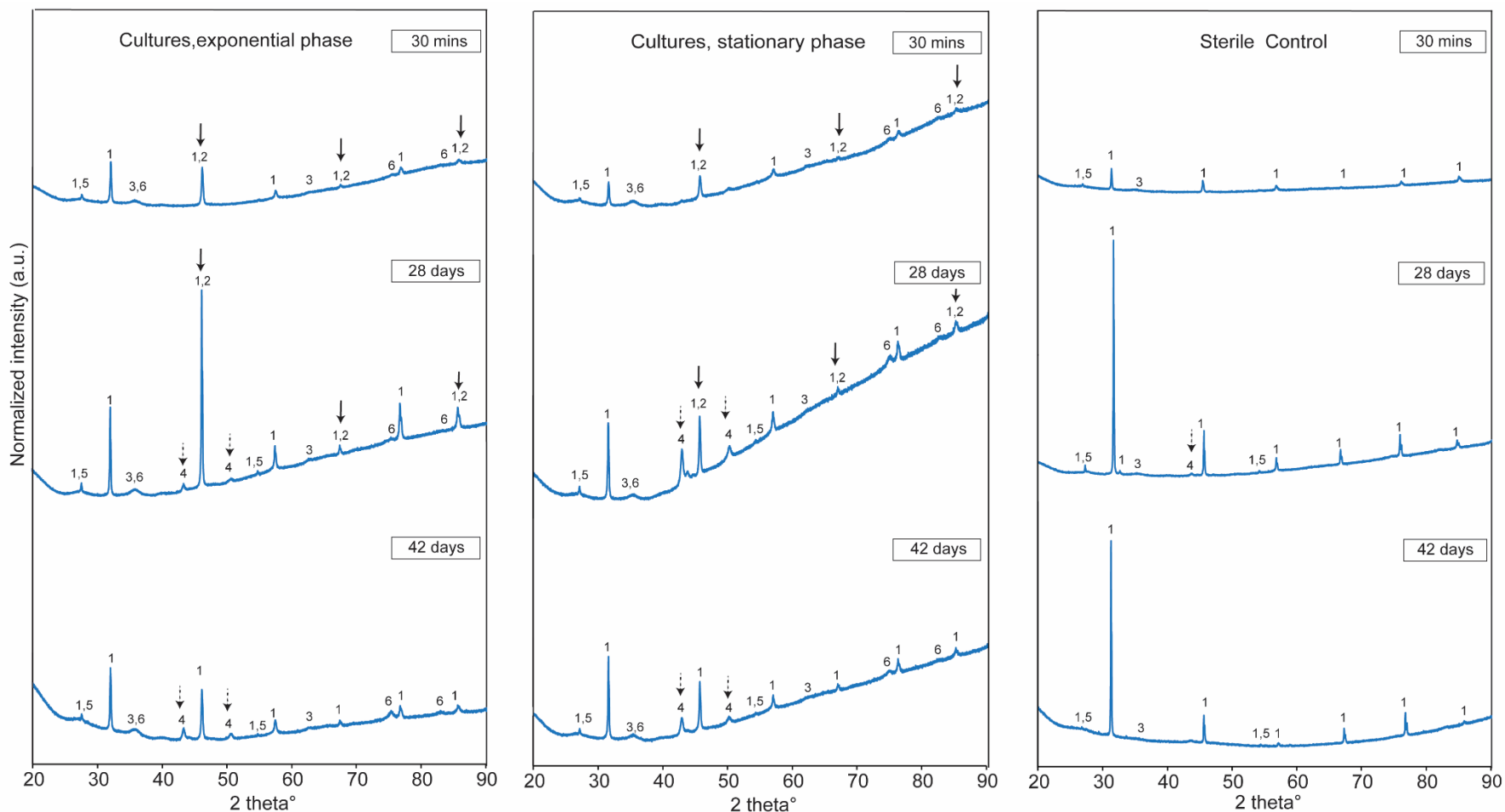


Figure S4: XRD spectra of minerals sampled from *M. barkeri* cultures in exponential phase (left column), *M. barkeri* cultures in stationary phase (middle column) and sterile controls (right column) in experimental series that tested the influence of headspace gas composition on mineral composition after the addition of ferrihydrite. The headspace gas remained as $\text{CH}_4/\text{H}_2/\text{CO}_2$ before the addition of ferrihydrite. The medium was reduced by Ti(III)-citrate and contained 1 g/L of organic additives. The samples were collected at 30 mins, 28 days and 42 days after the addition of ferrihydrite. XRD peak assignments: (1) Halite (NaCl); (2) Ferrite [$\alpha\text{-Fe}(0)$]; (3) Ferrihydrite (Fe_2O_3); (4) Austenite [$\gamma\text{-Fe}(0)$]; (5) Rutile (TiO_2); and (6) Titanomagnetite ($\text{Ti}_2\text{Fe}_3\text{O}_4$).

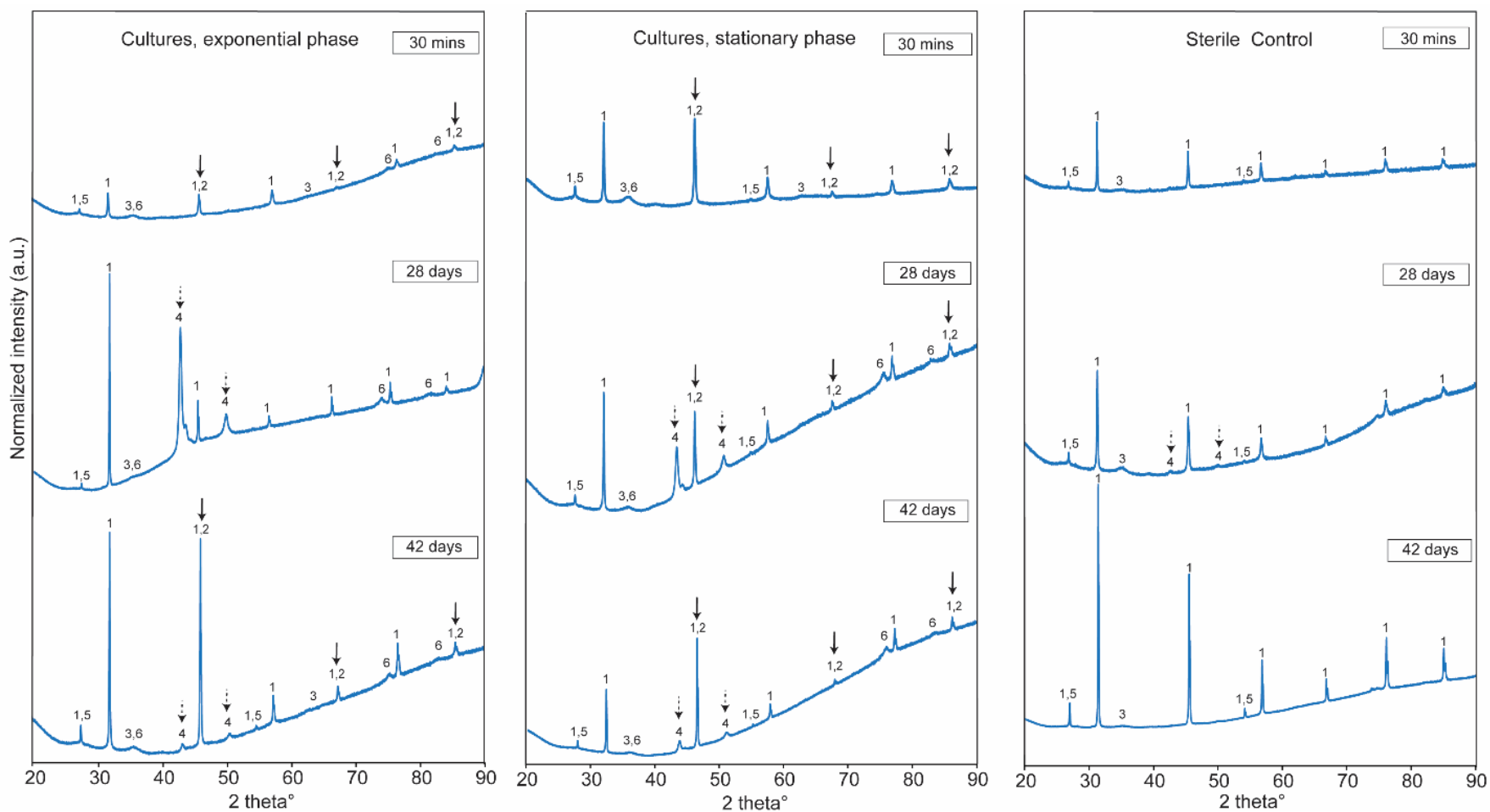


Figure S5: XRD spectra of minerals sampled from *M. barkeri* cultures in exponential phase (left column), *M. barkeri* cultures in stationary phase (middle column) and sterile controls (right column) in experimental series that tested the influence of the content of organic additives on mineral composition after the addition of ferrihydrite. The medium contained 4 g/L of organic additives and was reduced by Ti(III)-citrate and the headspace gas was replaced by N₂/CO₂ before the addition of ferrihydrite. The samples were collected at 30 mins, 28 days and 42 days after the addition of ferrihydrite. XRD peak assignments: (1) Halite (NaCl); (2) Ferrite [α -Fe(0)]; (3) Ferrihydrite (Fe₂O₃); (4) Austenite [γ -Fe(0)]; (5) Rutile (TiO₂); and (6) Titanomagnetite (Ti₂Fe₃O₄).

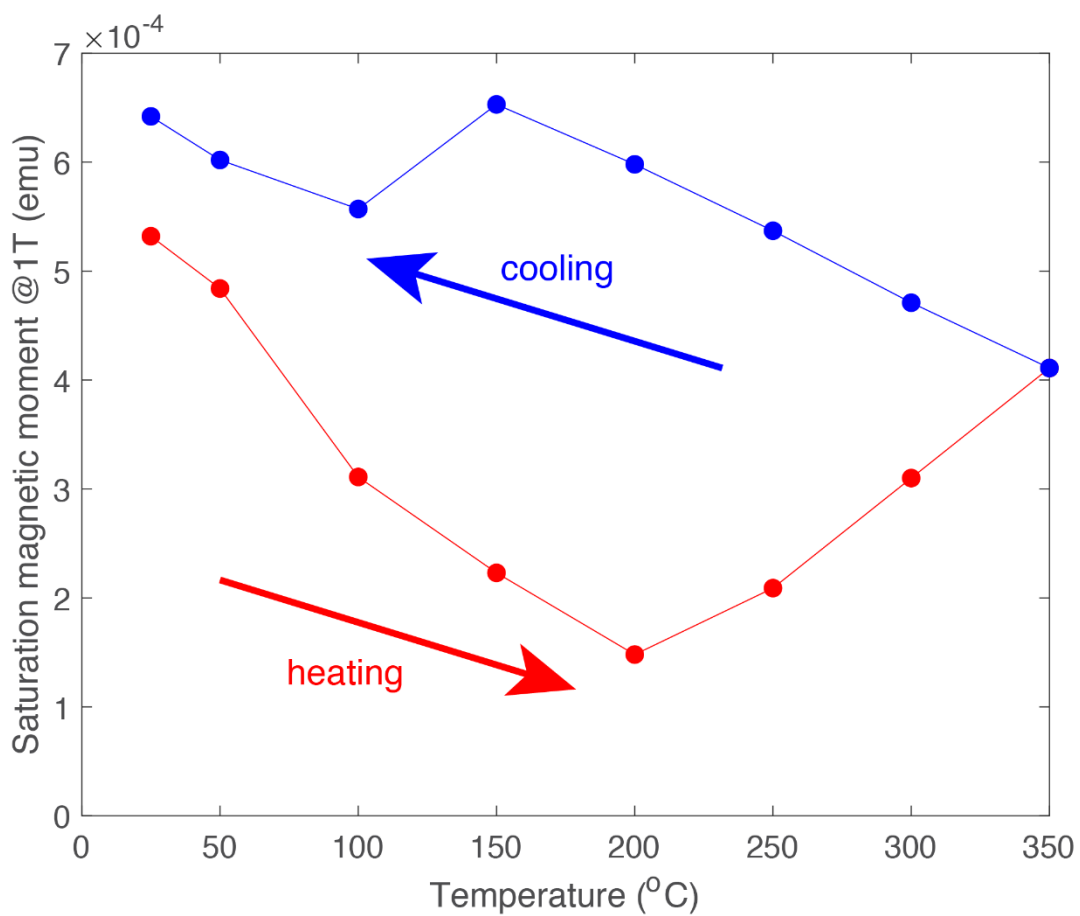


Figure S6: Thermomagnetic measurements showing saturation magnetic moment, at 1 T, as a function of the temperature, with heating (red) and cooling (blue) cycles. Cooling and heating curves do not overlay indicating alteration during the experiments. As a result, our attempts to quantify ZVI using thermomagnetic measurements did not succeed.

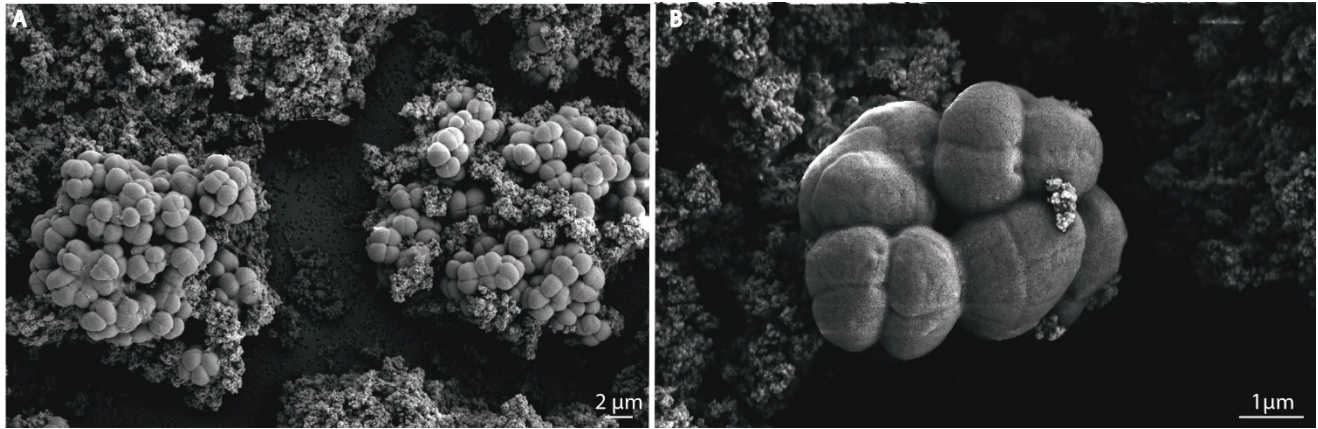


Figure S7: SEM images of *M. barkeri* cultures and minerals before the addition of ferrihydrite. (A) Large aggregates of coccus-shaped *M. barkeri*. (B) A cluster of *M. barkeri* showing flat surfaces.

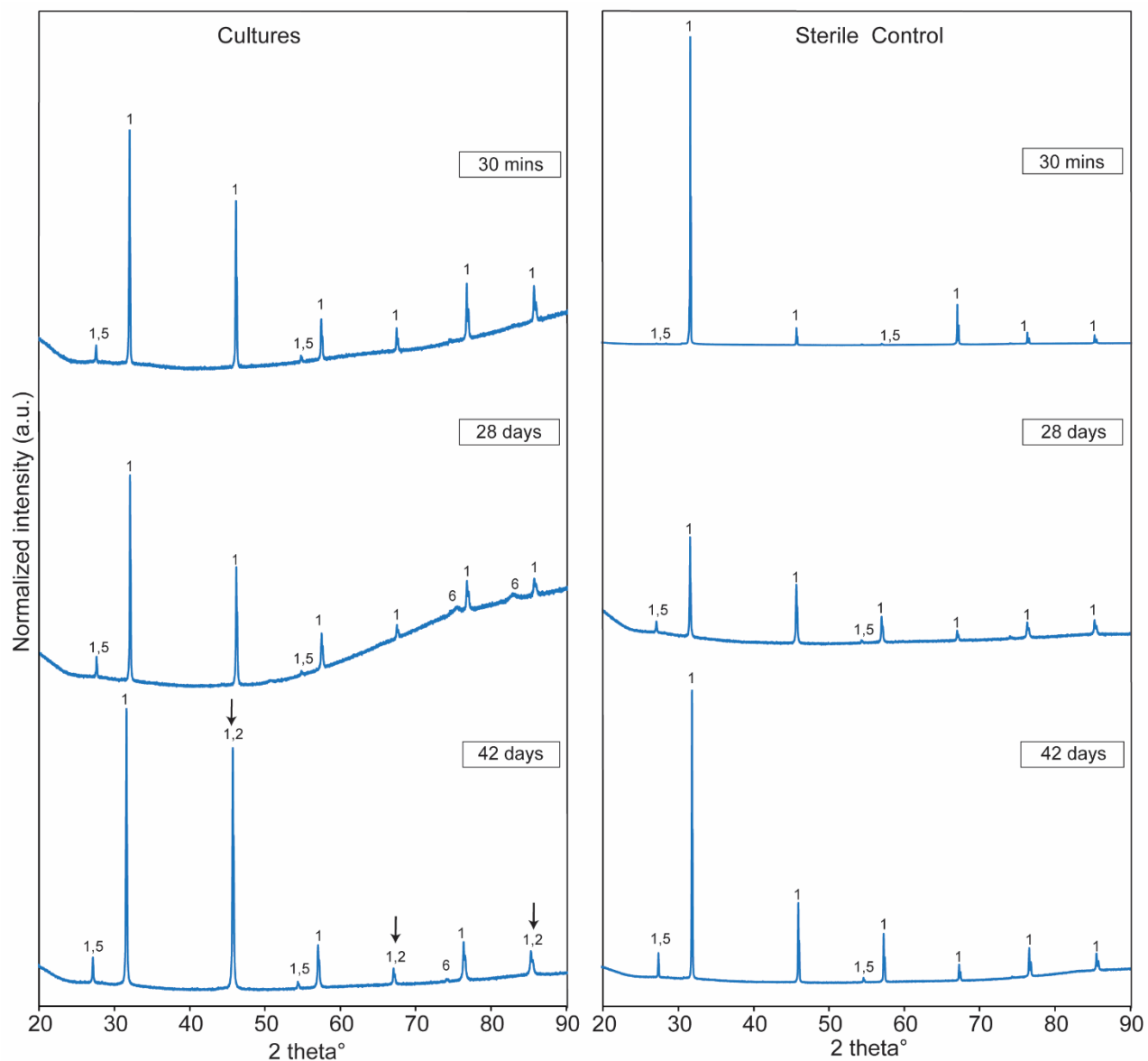


Figure S8: XRD spectra of minerals sampled from *M. barkeri* cultures (left column) and sterile controls (right column) in the experimental series that tested the influence of Fe(III) source on mineral composition after the addition of ferrihydrite. FeCl₃ solution was used as the source of Fe(III). The medium was reduced by Ti(III)-citrate and contained 1 g/L of organic additives and the headspace gas was replaced by N₂/CO₂ before the addition of FeCl₃ solution in exponential phase. The samples were collected at 30 mins, 28 days and 42 days after the addition of ferrihydrite. XRD peak assignments: (1) Halite (NaCl); (2) Ferrite [α -Fe(0)]; (5) Rutile (TiO₂); and (6) Titanomagnetite (Ti₂Fe₃O₄).

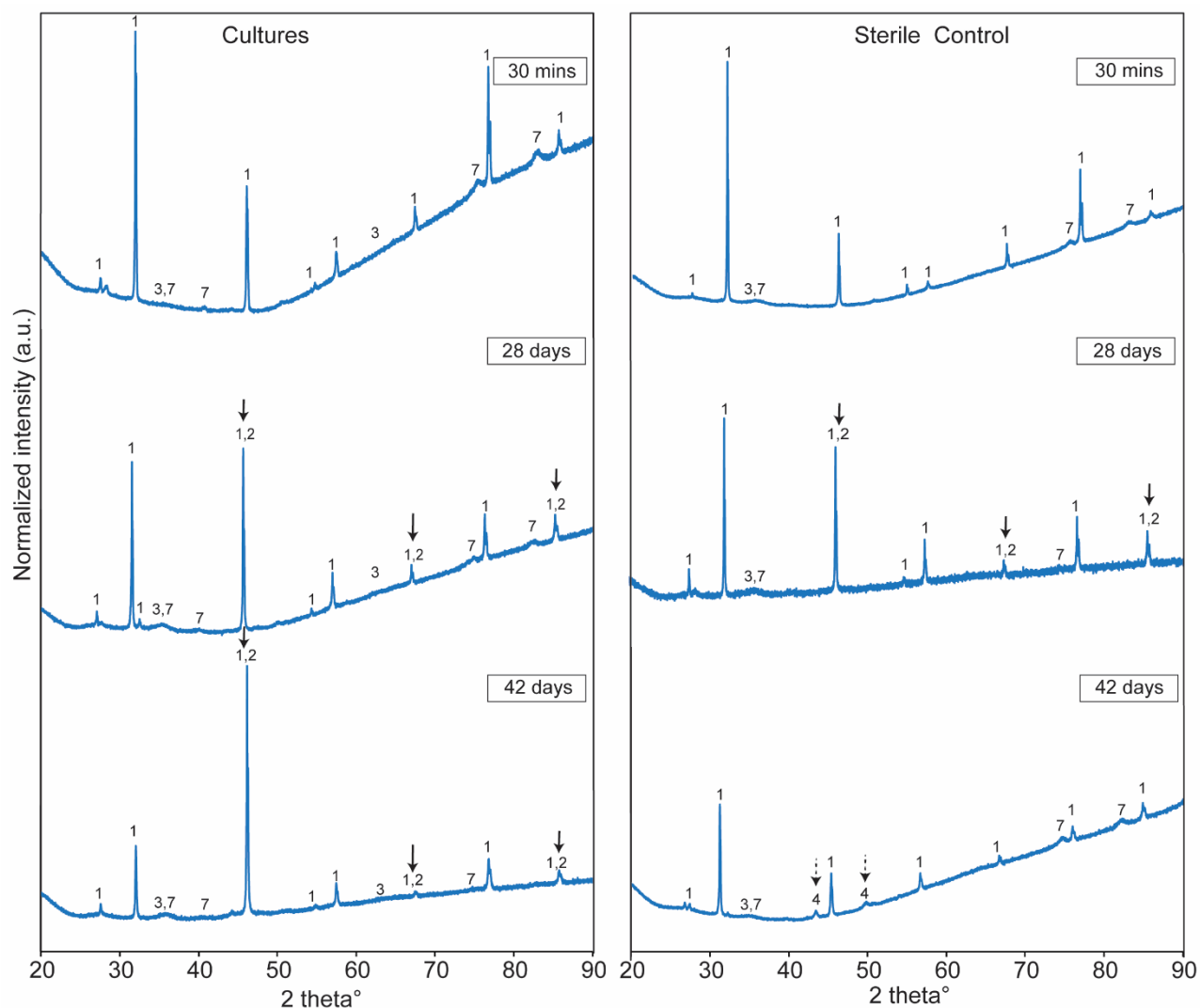


Figure S9: XRD spectra of minerals sampled from *M. barkeri* cultures (left column) and sterile controls (right column) that tested the influence of reducing agent on mineral composition after the addition of ferrihydrite. L-cysteine was added in medium as the reducing agent before the inoculation of *M. barkeri* cultures. The medium contained 1 g/L of organic additives and the headspace gas was replaced by N₂/CO₂ before the addition of ferrihydrite in exponential phase. The samples were collected at 30 mins, 28 days and 42 days after the addition of ferrihydrite. XRD peak assignments: (1) Halite (NaCl); (2) Ferrite [α -Fe(0)]; (3) Ferrihydrite (Fe₂O₃); (4) Austenite [γ -Fe(0)]; and (7) Magnetite (Fe₃O₄).

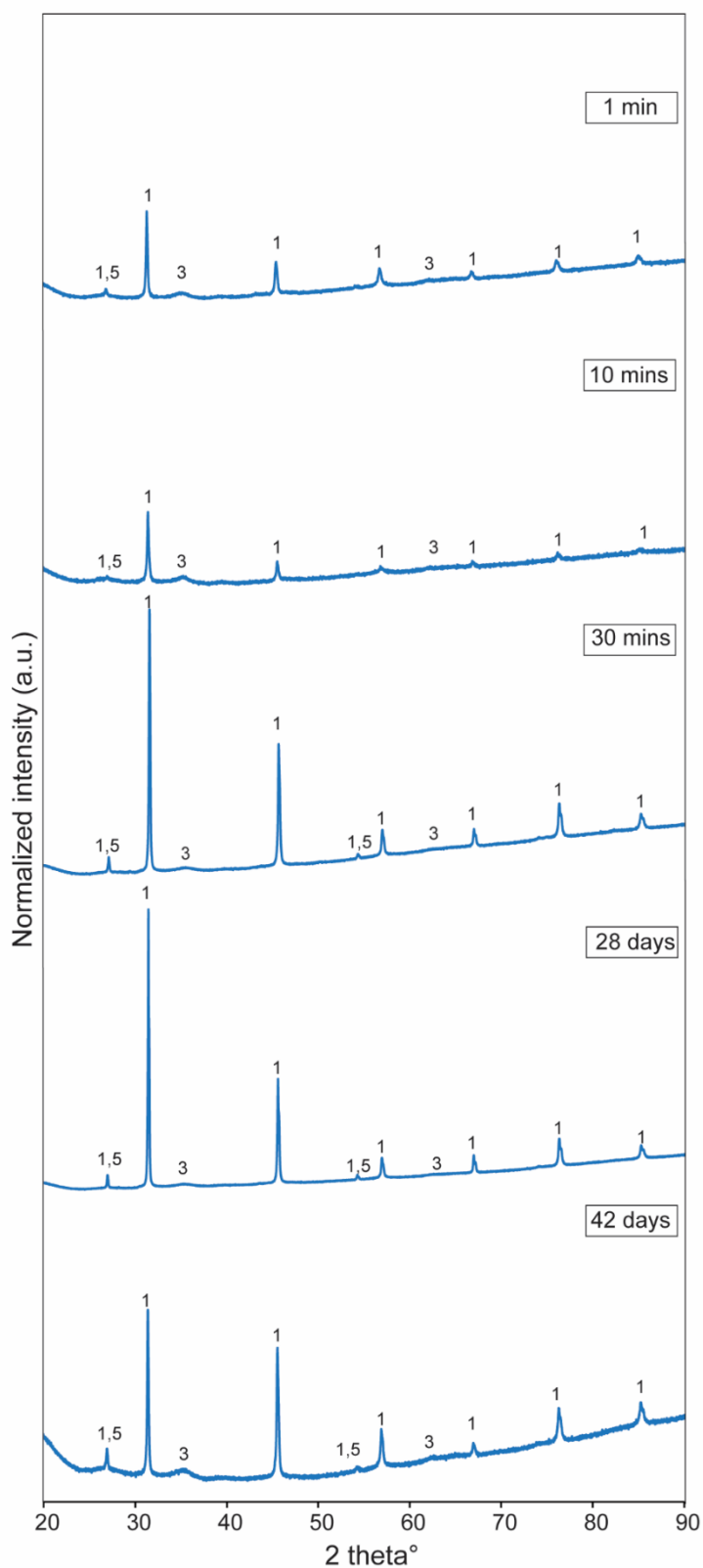


Figure S10: XRD spectra of minerals sampled from sterile controls of the cell-filtrate separation experiment. The medium did not contain organic additives and was reduced by Ti(III)-citrate and the headspace gas was replaced by N_2/CO_2 before the addition of ferrihydrite in exponential phase. The samples were collected at 1 min, 10mins, 30 mins, 28 days and 42 days after the addition of ferrihydrite. XRD peak assignments: (1) Halite (NaCl); (3) Ferrihydrite (Fe_2O_3); and (5) Rutile (TiO_2).

Table S3.1 Refined unit-cell parameters of the XRD spectra of samples from *M. barkeri* cells in organic-free medium (Figure 5) using Rietveld analyses

	Phase	Percentage (%)	Unit cell (Å)	d-spacing (Å)	Formula
1 min	Halite	30.2	a= 5.6440 b= 5.6440 c= 5.6440	2.8210	NaCl
	Ferrite	61.3	a= 2.8274 b= 2.8274 c= 2.8274	1.9901	α -Fe(0)
	Ferrihydrite	5.3	a= 4.8230 b= 5.0090 c= 7.1610	2.49339	Fe ₂ O ₃
	Rutile	2.2	a= 4.9530 b= 4.9530 c= 2.9590	3.24800	TiO ₂
	Titanomagnetite	1.2	a= 8.4689 b= 8.4689 c= 8.4689	2.55437	Ti ₂ Fe ₃ O ₄
5 mins	Halite	52.7	a= 5.6440 b= 5.6440 c= 5.6440	2.8210	NaCl
	Ferrite	32.5	a= 2.8274 b= 2.8274 c= 2.8274	1.9901	α -Fe(0)
	Ferrihydrite	8.2	a= 4.8230 b= 5.0090 c= 7.1610	2.49339	Fe ₂ O ₃
	Rutile	3.2	a= 4.9530 b= 4.9530 c= 2.9590	3.24800	TiO ₂
	Titanomagnetite	3.4	a= 8.4689 b= 8.4689 c= 8.4689	2.55437	Ti ₂ Fe ₃ O ₄
10 mins	Halite	54.6	a= 5.6440 b= 5.6440 c= 5.6440	2.8210	NaCl
	Ferrihydrite	9.3	a= 4.8230 b= 5.0090 c= 7.1610	2.49339	Fe ₂ O ₃
	Ferrite	28.7	a= 2.8274 b= 2.8274 c= 2.8274	1.9901	α -Fe(0)
	Rutile	3.2	a= 4.9530 b= 4.9530 c= 2.9590	3.24800	TiO ₂

30 mins	Titanomagnetite	4.2	a= 8.4689 b= 8.4689 c= 8.4689	2.55437	Ti ₂ Fe ₃ O ₄
	Halite	57.6	a= 5.6440 b= 5.6440 c= 5.6440	2.8210	NaCl
	Ferrihydrite	9.8	a= 4.8230 b= 5.0090 c= 7.1610	2.49339	Fe ₂ O ₃
	Rutile	3.2	a= 4.9530 b= 4.9530 c= 2.9590	3.24800	TiO ₂
	Ferrite	25.9	a= 2.8274 b= 2.8274 c= 2.8274	1.9901	α-Fe(0)
	Titanomagnetite	3.5	a= 8.4689 b= 8.4689 c= 8.4689	2.55437	Ti ₂ Fe ₃ O ₄
14 days	Halite	70.1	a= 5.6440 b= 5.6440 c= 5.6440	2.8210	NaCl
	Ferrihydrite	14.8	a= 4.8230 b= 5.0090 c= 7.1610	2.49339	Fe ₂ O ₃
	Rutile	4.2	a= 4.9530 b= 4.9530 c= 2.9590	3.24800	TiO ₂
	Titanomagnetite	10.9	a= 8.4689 b= 8.4689 c= 8.4689	2.55437	Ti ₂ Fe ₃ O ₄
28 days	Halite	73.2	a= 5.6440 b= 5.6440 c= 5.6440	2.8210	NaCl
	Ferrihydrite	12.9	a= 4.8230 b= 5.0090 c= 7.1610	2.49339	Fe ₂ O ₃
	Rutile	4.3	a= 4.9530 b= 4.9530 c= 2.9590	3.24800	TiO ₂
	Titanomagnetite	9.6	a= 8.4689 b= 8.4689 c= 8.4689	2.55437	Ti ₂ Fe ₃ O ₄
42 days	Halite	69.3	a= 5.6440 b= 5.6440 c= 5.6440	2.8210	NaCl

Ferrihydrite	25.5	a= 4.8230 b= 5.0090 c= 7.1610	2.49339	Fe ₂ O ₃
Rutile	3.9	a= 4.9530 b= 4.9530 c= 2.9590	3.24800	TiO ₂
Titanomagnetite	1.3	a= 8.4689 b= 8.4689 c= 8.4689	2.55437	Ti ₂ Fe ₃ O ₄

Table S3.2 Refined unit-cell parameters of the XRD spectra of samples from filter-sterilized spent supernatants (Figure 5) using Rietveld analyses

	Phase	Percentage (%)	Unit cell (Å)	d-spacing (Å)	Formula
1 min	Halite	61.7	a= 5.6440 b= 5.6440 c= 5.6440	2.8210	NaCl
	Ferrite	25.6	a= 2.8274 b= 2.8274 c= 2.8274	1.9901	α -Fe(0)
	Ferrihydrite	10.1	a= 4.8230 b= 5.0090 c= 7.1610	2.49339	Fe ₂ O ₃
	Rutile	2.4	a= 4.9530 b= 4.9530 c= 2.9590	3.24800	TiO ₂
	Titanomagnetite	0.2	a= 8.4689 b= 8.4689 c= 8.4689	2.55437	Ti ₂ Fe ₃ O ₄
5 mins	Halite	53.6	a= 5.6440 b= 5.6440 c= 5.6440	2.8210	NaCl
	Ferrite	34.1	a= 2.8274 b= 2.8274 c= 2.8274	1.9901	α -Fe(0)
	Ferrihydrite	8.2	a= 4.8230 b= 5.0090 c= 7.1610	2.49339	Fe ₂ O ₃
	Rutile	2.6	a= 4.9530 b= 4.9530 c= 2.9590	3.24800	TiO ₂
	Titanomagnetite	1.5	a= 8.4689 b= 8.4689 c= 8.4689	2.55437	Ti ₂ Fe ₃ O ₄
10 mins	Halite	44.6	a= 5.6440 b= 5.6440 c= 5.6440	2.8210	NaCl
	Ferrihydrite	6.1	a= 4.8230 b= 5.0090 c= 7.1610	2.49339	Fe ₂ O ₃
	Ferrite	38.7	a= 2.8274 b= 2.8274 c= 2.8274	1.9901	α -Fe(0)
	Rutile	3.4	a= 4.9530 b= 4.9530 c= 2.9590	3.24800	TiO ₂

30 mins	Titanomagnetite	7.2	a= 8.4689 b= 8.4689 c= 8.4689	2.55437	Ti ₂ Fe ₃ O ₄
	Halite	34.6	a= 5.6440 b= 5.6440 c= 5.6440	2.8210	NaCl
	Ferrihydrite	5.3	a= 4.8230 b= 5.0090 c= 7.1610	2.49339	Fe ₂ O ₃
	Rutile	3.7	a= 4.9530 b= 4.9530 c= 2.9590	3.24800	TiO ₂
	Ferrite	53.2	a= 2.8274 b= 2.8274 c= 2.8274	1.9901	α-Fe(0)
	Titanomagnetite	3.2	a= 8.4689 b= 8.4689 c= 8.4689	2.55437	Ti ₂ Fe ₃ O ₄
14 days	Halite	59.9	a= 5.6440 b= 5.6440 c= 5.6440	2.8210	NaCl
	Ferrihydrite	15.4	a= 4.8230 b= 5.0090 c= 7.1610	2.49339	Fe ₂ O ₃
	Rutile	4.1	a= 4.9530 b= 4.9530 c= 2.9590	3.24800	TiO ₂
	Austenite	17.8	a= 3.6000 b= 3.6000 c= 3.6000	2.07846	γ-Fe(0)
	Titanomagnetite	2.8	a= 8.4689 b= 8.4689 c= 8.4689	2.55437	Ti ₂ Fe ₃ O ₄
	Halite	65.4	a= 5.6440 b= 5.6440 c= 5.6440	2.8210	NaCl
28 days	Ferrihydrite	18.4	a= 4.8230 b= 5.0090 c= 7.1610	2.49339	Fe ₂ O ₃
	Rutile	3.8	a= 4.9530 b= 4.9530 c= 2.9590	3.24800	TiO ₂
	Austenite	10.2	a= 3.6000 b= 3.6000 c= 3.6000	2.07846	γ-Fe(0)

42 days	Titanomagnetite	2.2	a= 8.4689 b= 8.4689 c= 8.4689	2.55437	Ti ₂ Fe ₃ O ₄
	Halite	69	a= 5.6440 b= 5.6440 c= 5.6440	2.8210	NaCl
	Ferrihydrite	26.5	a= 4.8230 b= 5.0090 c= 7.1610	2.49339	Fe ₂ O ₃
	Rutile	4.1	a= 4.9530 b= 4.9530 c= 2.9590	3.24800	TiO ₂
	Titanomagnetite	0.4	a= 8.4689 b= 8.4689 c= 8.4689	2.55437	Ti ₂ Fe ₃ O ₄

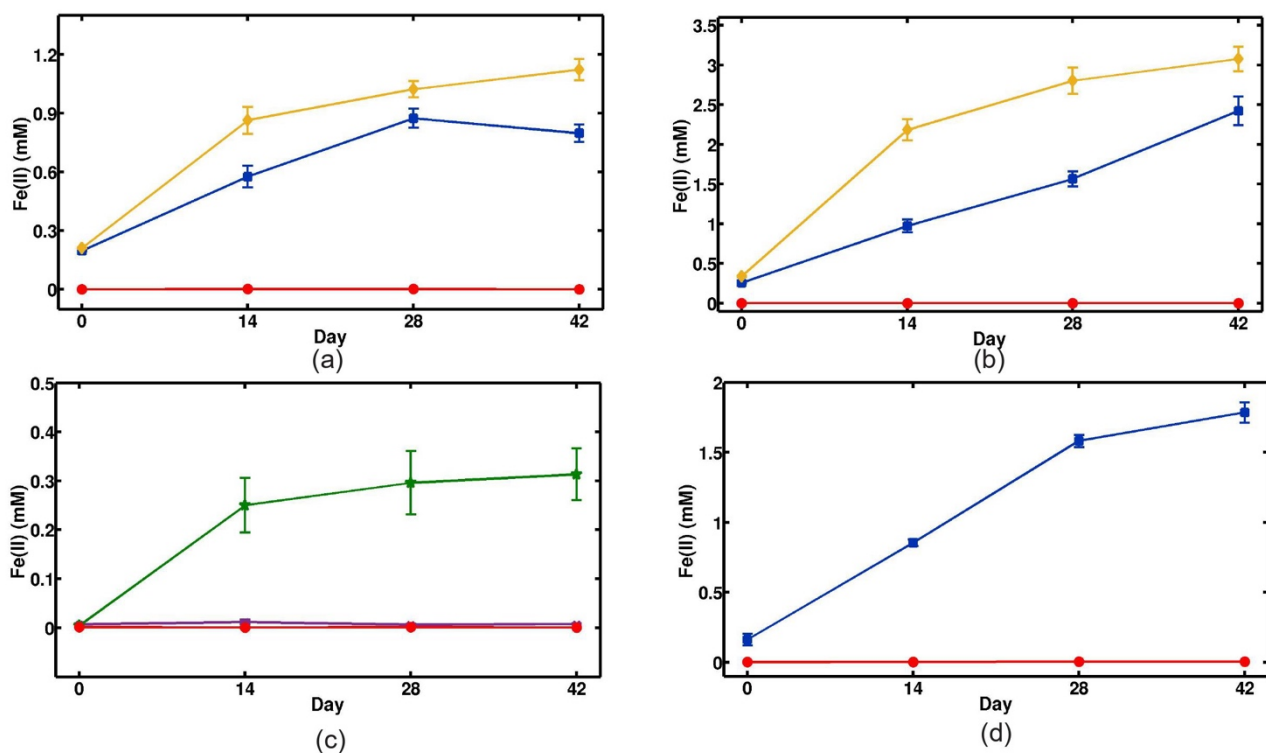


Figure S11: Fe(II) concentration in *M. barkeri* cultures and sterile controls. All media were reduced by Ti(III)-citrate. (a) 1 g/L of organic additives with CH₄/H₂/CO₂ in the headspace, ferrihydrite as the iron source. (b) 4 g/L of organic additives with N₂/CO₂ in the headspace, ferrihydrite as the iron source. (c) 1 g/L of organic additives and N₂/CO₂ in the headspace, ferrihydrite as the iron source. Before the addition of ferrihydrite, both filter-sterilized spent supernatants and *M. barkeri* cells in organic-free medium were heated at 120 °C in an oven for 4 hours in an oven and allowed to cool at room temperature (20 °C) for 5 hours. (d) 1 g/L of organic additives and N₂/CO₂ in the headspace, FeCl₃ as the iron source. In (a), (b), (c) and (d), blue line and squares show measurements in *M. barkeri* cultures to which ferrihydrite was added in exponential phase, yellow line and diamonds show measurements in the cultures to which ferrihydrite was added in stationary phase, red line and circles show measurements in sterile controls, purple line and crosses show Fe(II) concentrations in cell suspensions in organic-free medium, and green line and stars show Fe(II) concentrations in filter-sterilized spent supernatants. Each point shows the average concentration from triplicate bottles and the error bar shows the standard deviation.

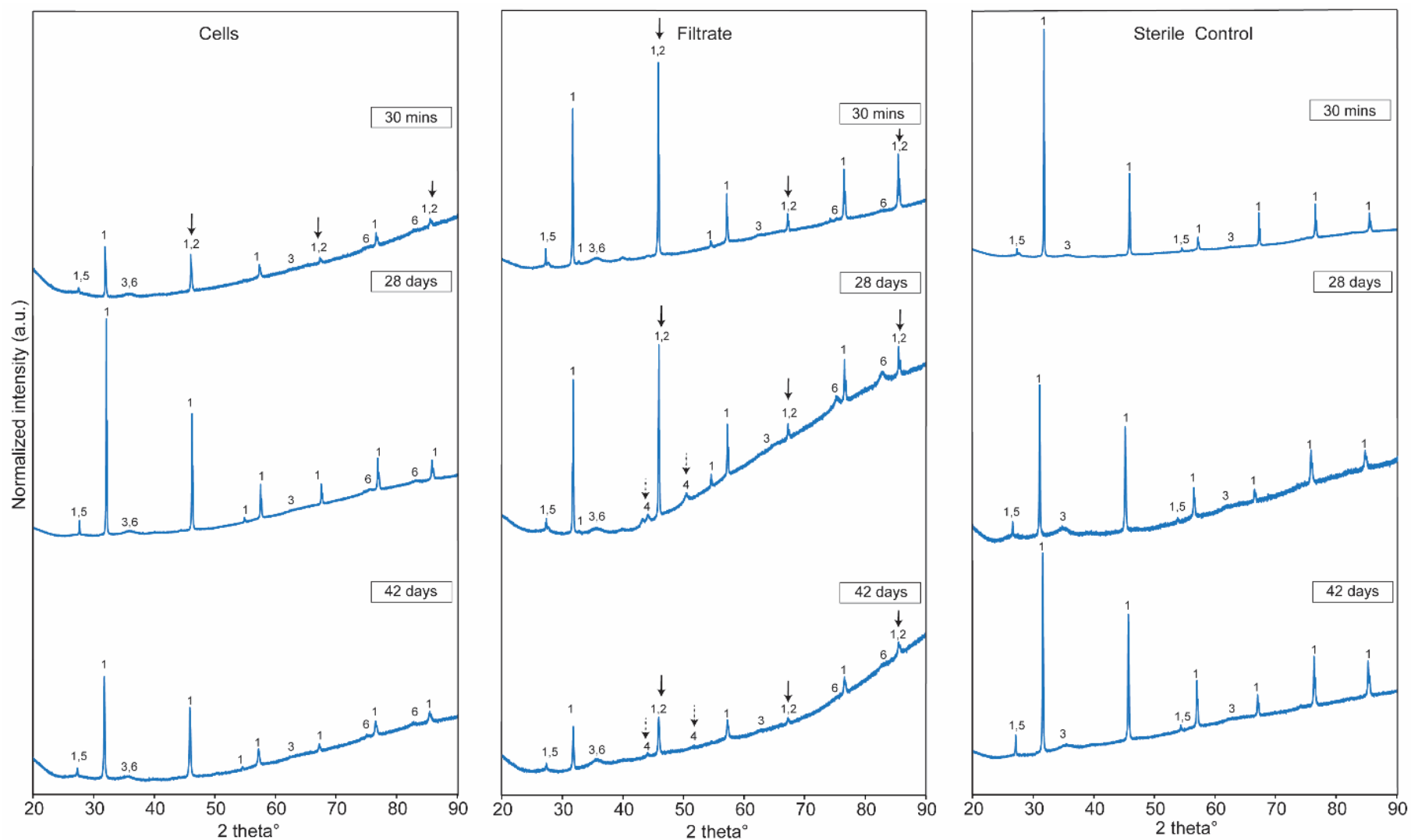


Figure S12: XRD spectra of minerals sampled from *M. barkeri* cells in organic-free medium (left column), filter-sterilized spent supernatants (middle column) and organic-free sterile controls (right column) in the experimental series that tested if the formation of Fe(0) requires some enzymatic activity. Before the addition of ferrihydrite, *M. barkeri* cells in organic-free medium, filter-sterilized spent supernatants and sterile controls were all heated at 120 °C in an oven for 4 hours and were allowed to cool at room temperature for 5 hours. The medium was reduced by Ti(III)-citrate and the headspace gas was replaced by N₂/CO₂ before the addition of ferrihydrite. The samples were collected at 30 mins, 28 days and 42 days after the addition of ferrihydrite. XRD peak assignments: (1) Halite (NaCl); (2) Ferrite [α -Fe(0)]; (3) Ferrihydrite (Fe₂O₃); (4) Austenite [γ -Fe(0)]; (5) Rutile (TiO₂); and (6) Titanomagnetite (Ti₂Fe₃O₄).